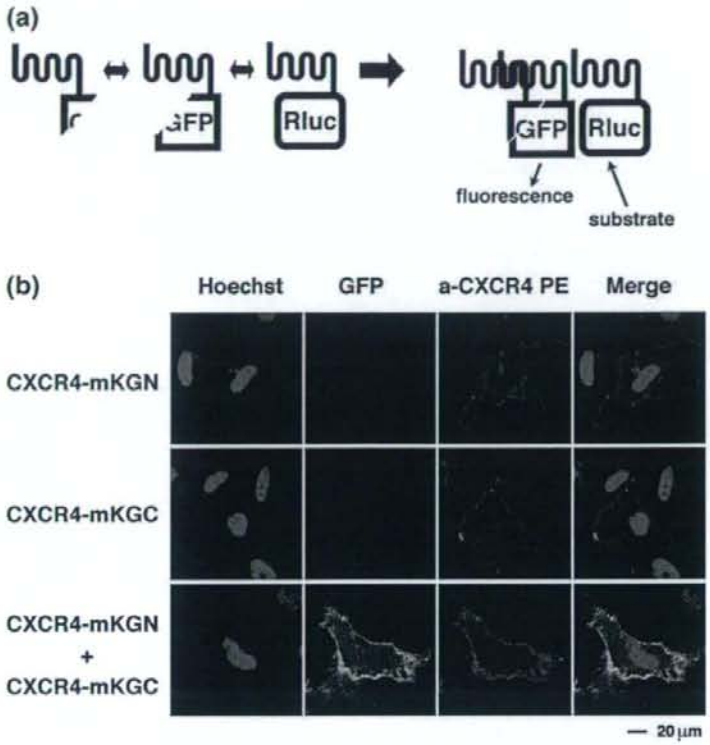

Fig. 5. Bioluminescent resonance energy transfer (BRET)–bimolecular fluorescence complementation (BiFC) analysis to demonstrate the presence of a higher-order molecular clustering of CXCR4. (a) Schematic drawing of the BiFC–BRET assay system. The bioluminescence energy from renilla luciferase (Rluc) was absorbed by green fluorescent protein (GFP; mKG) reconstituted by amino- and carboxy-terminal fragments to emit green fluorescence. (b) Detection of a BiFC signal by coexpressing CXCR4-mKGN and CXCR-mKGC. Cell surface expression of CXCR4-mKGN and CXCR4-mKGC was detected by an immunofluorescence assay using anti-CXCR4 R-phycoerythrin (PE) (a-CXCR4 R-phycoerythrin). The green fluorescence was detected only when two constructs were cointroduced into cells (bottom). Green, red, and blue represent GFP, PE, and the Hoechst 33258-stained nucleus, respectively. Magnification, ×630; scale bar = 20 μm.

(Table 4). These data indicate that the BiFC–BRET signal is specific for CXCR4, and that CXCR4 forms a molecular complex consisting of more than two molecules *in vivo*. The BiFC–BRET signals were lower than the BRET signals, presumably because of the decreased efficiencies of green fluorescence activation by mKGN and mKGC fragments relative to full-length GFP. Taken together, our *in vivo* biophysical analysis favors a multimerization model for CXCR4.

Discussion

In the present work, we demonstrated that CXCR4 forms a complex consisting of more than two molecules (a multimer) in the absence of CXCL12/SDF-1α by using a combination of BRET and BiFC techniques. The BiFC–BRET approach is a powerful technique for directly identifying a trimolecular complex in living cells, and may be applied to other protein–protein interactions.

Any application of FRET or BRET techniques to GPCR has to be done carefully, as GPCR often yield significant background signals.[41] The use of comparative studies with other GPCR, including CXCR2, CXCR3, and CCR5, as well as the careful monitoring of GFP and Rluc expression levels, allowed us to obtain compelling evidence for a specific homotypic interaction of CXCR4. The technical limitation of BiFC–BRET is that it is not possible to determine how many molecules are involved in the higher-order complex. To further characterize the molecular assembly, it will be necessary to develop a system that yields signals only when a target molecule tetramerizes.

We demonstrated that the higher-order clusterization of CXCR4 was not mediated by the amino- or carboxy-termini but by multiple TMD, consistent with the GPCR oligomerization models. However, we were unable to determine the TMD pairs that contribute most to CXCR4 multimerization. Consequently, we failed to isolate monomeric CXCR4. Treating cells with the CXCR4 ligand CXCL12/SDF-1α at cell migration-inducing concentrations did not increase BRET levels (data not shown), also suggesting the presence of higher-order CXCR4 clusters under steady-state conditions. This type of preformed receptor multimerization has been documented for receptors such as CCR5.[28] The biological advantage of CXCR4 assembly is its effective ability to 'radar' CXCL12/SDF-1α in the microenvironment for the induction of cell migration or targeted metastasis of cancer cells.[42,43] Steady-state multimerization is important because a molecular cluster would increase avidity for CXCL12/SDF-1α. We assume that high sensitivity for the ligand is critical for normal and malignant cells to be able to determine which direction to migrate to in in response to ligand stimulation.

CXCR4 does not display apparent punctate signals on the cell surface, as visualized by GFP tagging or immunostaining, even though our data predict that CXCR4 multimerizes. This suggests that only a limited number of CXCR4 molecules might participate in a multimeric unit. Bovine rhodopsin has been demonstrated to form a higher-order structure characterized by dimer arrays.[44] Given the structural similarities among GPCR, the basic unit of the higher-order cluster of CXCR4 may also be a dimer. It is possible that a pair of dimers forms a CXCR4 tetramolecular complex. These hypothetical models may be probed further using atomic force microscopy.

As shown in Figure 5b, the expression of CXCR4-mKGN and CXCR4-mKGC yielded green fluorescence at the cell periphery. This is compelling evidence that CXCR4 multimerizes at the cell surface. CXCR4 does not actively form a complex in the ER

but does so in the post-ER-to-Golgi compartments as suggested by the following data. When 293T cells expressing CXCR4-GFP and CXCR4-Rluc were treated with brefeldin A, which blocks the transport of proteins from the ER to post-Golgi compartments, the BRET levels dropped substantially to $63.7 \pm 15.2\%$ ($n = 7$) at 4 h after exposure. This drop in BRET level corresponded to the decrease in cell surface CXCR4 levels, even though the GFP and Rluc levels were unchanged (data not shown). Thus, it is unlikely that multimerization is required for CXCR4 to egress from the ER. CXCR4 may start to oligomerize in post-ER compartments and probably play a role at the cell surface, as hypothesized above. We believe that it will be informative to study how CXCR4 oligomerization is prohibited in the ER. By knowing this, we may be able to design novel CXCR4 inhibitors that disassemble the CXCR4 multimer. BiFC–BRET-based biophysical analyses would be a powerful tool for further studies.

Acknowledgments

We thank Dr Tsutomu Murakami for critically reading the manuscript. This work was partly supported by the Japan Health Science Foundation, the Japanese Ministry of Health, Labor and Welfare (H18-AIDS-W-003), and the Japanese Ministry of Education, Culture, Sports, Science, and Technology (18689014 and 18659136).

References

1 Gupta SK, Lysko PG, Pillarisetti K *et al.* Chemokine receptors in human endothelial cells. Functional expression of CXCR4 and its transcriptional regulation by inflammatory cytokines. *J Biol Chem* 1998; **273**: 4282–7.
2 Li S, Huang S, Peng SB. Overexpression of G protein-coupled receptors in cancer cells: involvement in tumor progression. *Int J Oncol* 2005; **27**: 1329–39.
3 Balabanian K, Lagane B, Pablos JL *et al.* WHIM syndromes with different genetic anomalies are accounted for by impaired CXCR4 desensitization to CXCL12. *Blood* 2005; **105**: 2449–57.
4 Gulino AV, Moratto D, Sozzani S *et al.* Altered leukocyte response to CXCL12 in patients with warts hypogammaglobulinemia, infections, myelokathexis (WHIM) syndrome. *Blood* 2004; **104**: 444–52.
5 Hernandez PA, Gorlin RJ, Lukens JN *et al.* Mutations in the chemokine receptor gene *CXCR4* are associated with WHIM syndrome, a combined immunodeficiency disease. *Nat Genet* 2003; **34**: 70–4.
6 Zou YR, Kottmann AH, Kuroda M, Taniuchi I, Littman DR. Function of the chemokine receptor CXCR4 in haematopoiesis and in cerebellar development. *Nature* 1998; **393**: 595–9.
7 Feng Y, Broder CC, Kennedy PE, Berger EA. HIV-1 entry cofactor: functional cDNA cloning of a seven-transmembrane, G protein-coupled receptor. *Science* 1996; **272**: 872–7.
8 Koizumi K, Hojo S, Akashi T, Yasumoto K, Saiki I. Chemokine receptors in cancer metastasis and cancer cell-derived chemokines in host immune response. *Cancer Sci* 2007; **98**: 1652–8.
9 Arya M, Ahmed H, Silhi N, Williamson M, Patel HR. Clinical importance and therapeutic implications of the pivotal CXCL12–CXCR4 (chemokine ligand–receptor) interaction in cancer cell migration. *Tumour Biol* 2007; **28**: 123–31.
10 Raman D, Baugher PJ, Thu YM, Richmond A. Role of chemokines in tumor growth. *Cancer Lett* 2007; **256**: 137–65.
11 Billadeau DD, Chatterjee S, Bramati P *et al.* Characterization of the CXCR4 signaling in pancreatic cancer cells. *Int J Gastrointest Cancer* 2006; **37**: 110–19.
12 Akashi T, Koizumi K, Tsuneyama K, Saiki I, Takano Y, Fuse H. Chemokine receptor CXCR4 expression and prognosis in patients with metastatic prostate cancer. *Cancer Sci* 2008; **99**: 539–42.
13 Yang S, Pham LK, Liao CP, Frenkel B, Reddi AH, Roy-Burman P. A novel bone morphogenetic protein signaling in heterotypic cell interactions in prostate cancer. *Cancer Res* 2008; **68**: 198–205.
14 De Falco V, Guarino V, Avilla E *et al.* Biological role and potential therapeutic targeting of the chemokine receptor CXCR4 in undifferentiated thyroid cancer. *Cancer Res* 2007; **67**: 11 821–9.
15 Tucci MG, Lucarini G, Brancorsini D *et al.* Involvement of E-cadherin, beta-catenin, Cdc42 and CXCR4 in the progression and prognosis of cutaneous melanoma. *Br J Dermatol* 2007; **157**: 1212–16.
16 Kollmar O, Rupertus K, Scheuer C *et al.* Stromal cell-derived factor-1 promotes cell migration and tumor growth of colorectal metastasis. *Neoplasia* 2007; **9**: 862–70.
17 Holmes WD, Consler TG, Dallas WS, Rocque WJ, Willard DH. Solution studies of recombinant human stromal-cell-derived factor-1. *Protein Expr Purif* 2001; **21**: 367–77.
18 Veldkamp CT, Peterson FC, Pelzek AJ, Volkman BF. The monomer–dimer equilibrium of stromal cell-derived factor-1 (CXCL 12) is altered by pH, phosphate, sulfate, and heparin. *Protein Sci* 2005; **14**: 1071–81.
19 Baryshnikova OK, Sykes BD. Backbone dynamics of SDF-1α determined by NMR: interpretation in the presence of monomer–dimer equilibrium. *Protein Sci* 2006; **15**: 2568–78.
20 Babcock GJ, Farzan M, Sodroski J. Ligand-independent dimerization of CXCR4, a principal HIV-1 coreceptor. *J Biol Chem* 2003; **278**: 3378–85.
21 Vila-Coro AJ, Rodriguez-Frade JM, Martin De Ana A, Moreno-Ortiz MC, Martinez AC, Mellado M. The chemokine SDF-1α triggers CXCR4 receptor dimerization and activates the JAK/STAT pathway. *FASEB J* 1999; **13**: 1699–710.
22 Toth PT, Ren D, Miller RJ. Regulation of CXCR4 receptor dimerization by the chemokine SDF-1α and the HIV-1 coat protein gp120: a fluorescence resonance energy transfer (FRET) study. *J Pharmacol Exp Ther* 2004; **310**: 8–17.
23 Wang J, He L, Combs CA, Roderiquez G, Norcross MA. Dimerization of CXCR4 in living malignant cells: control of cell migration by a synthetic peptide that reduces homologous CXCR4 interactions. *Mol Cancer Ther* 2006; **5**: 2474–83.
24 Terrillon S, Bouvier M. Roles of G-protein-coupled receptor dimerization. *EMBO Rep* 2004; **5**: 30–4.
25 Milligan G. G protein-coupled receptor dimerization: function and ligand pharmacology. *Mol Pharmacol* 2004; **66**: 1–7.
26 Lee SP, O'Dowd BF, Rajaram RD, Nguyen T, George SR. D2 dopamine receptor homodimerization is mediated by multiple sites of interaction, including an intermolecular interaction involving transmembrane domain 4. *Biochemistry* 2003; **42**: 11 023–31.
27 Thevenin D, Lazarova T, Roberts MF, Robinson CR. Oligomerization of the fifth transmembrane domain from the adenosine A2A receptor. *Protein Sci* 2005; **14**: 2177–86.
28 Hernanz-Falcon P, Rodriguez-Frade JM, Serrano A *et al.* Identification of amino acid residues crucial for chemokine receptor dimerization. *Nat Immunol* 2004; **5**: 216–23.
29 Muller-Taubenberger A, Anderson KI. Recent advances using green and red fluorescent protein variants. *Appl Microbiol Biotechnol* 2007; **77**: 1–12.
30 Gandia J, Galino J, Amaral OB *et al.* Detection of higher-order G protein-coupled receptor oligomers by a combined BRET–BiFC technique. *FEBS Lett* 2008; **582**: 2979–84.
31 Futahashi Y, Komano J, Urano E *et al.* Separate elements are required for ligand-dependent and -independent internalization of metastatic potentiator CXCR4. *Cancer Sci* 2007; **98**: 373–9.
32 Doranz BJ, Orsini MJ, Turner JD *et al.* Identification of CXCR4 domains that support coreceptor and chemokine receptor functions. *J Virol* 1999; **73**: 2752–61.
33 Shimizu S, Urano E, Futahashi Y *et al.* Inhibiting lentiviral replication by HEXIM1, a cellular negative regulator of the CDK9/cyclin T complex. *AIDS* 2007; **21**: 575–82.
34 Tarasova NI, Stauber RH, Michejda CJ. Spontaneous and ligand-induced trafficking of CXC-chemokine receptor 4. *J Biol Chem* 1998; **273**: 15 883–6.
35 Gether U. Uncovering molecular mechanisms involved in activation of G protein-coupled receptors. *Endocr Rev* 2000; **21**: 90–113.
36 Trettel F, Di Bartolomeo S, Lauro C, Catalano M, Ciotti MT, Limatola C. Ligand-independent CXCR2 dimerization. *J Biol Chem* 2003; **278**: 40 980–8.
37 Ling K, Wang P, Zhao J *et al.* Five-transmembrane domains appear sufficient for a G protein-coupled receptor: functional five-transmembrane domain chemokine receptors. *Proc Natl Acad Sci USA* 1999; **96**: 7922–7.
38 Willett BJ, Adema K, Heveker N *et al.* The second extracellular loop of CXCR4 determines its function as a receptor for feline immunodeficiency virus. *J Virol* 1998; **72**: 6475–81.
39 Heroux M, Hogue M, Lemieux S, Bouvier M. Functional calcitonin gene-related peptide receptors are formed by the asymmetric assembly of a calcitonin receptor-like receptor homo-oligomer and a monomer of receptor activity-modifying protein-1. *J Biol Chem* 2007; **282**: 31 610–20.
40 Ip DT, Wong KB, Wan DC. Characterization of novel orange fluorescent protein cloned from cnidarian tube anemone *Cerianthus* sp. *Mar Biotechnol (NY)* 2007; **9**: 469–78.
41 Salahpour A, Masri B. Experimental challenge to a 'rigorous' BRET analysis of GPCR oligomerization. *Nat Meth* 2007; **4**: 599–600.
42 Wang J, Loberg R, Taichman RS. The pivotal role of CXCL12 (SDF-1)/CXCR4 axis in bone metastasis. *Cancer Metastasis Rev* 2006; **25**: 573–87.
43 Burger JA, Kipps TJ. CXCR4: a key receptor in the crosstalk between tumor cells and their microenvironment. *Blood* 2006; **107**: 1761–7.
44 Fotiadis D, Liang Y, Filipek S, Saperstein DA, Engel A, Palczewski K. Atomic-force microscopy: Rhodopsin dimers in native disc membranes. *Nature* 2003; **421**: 127–8.

doi: 10.1111/j.1349-7006.2008.00997.x

FEBS Letters 582 (2008) 4053–4058

Identification of the P-TEFb complex-interacting domain of Brd4 as an inhibitor of HIV-1 replication by functional cDNA library screening in MT-4 cells

Emiko Urano[a,b], Yumi Kariya[a], Yuko Futahashi[a], Reiko Ichikawa[a], Makiko Hamatake[a], Hidesuke Fukazawa[c], Yuko Morikawa[b], Takeshi Yoshida[d], Yoshio Koyanagi[d], Naoki Yamamoto[a], Jun Komano[a,*]

[a] *National Institute of Infectious Diseases, 1-23-1 Toyama, Shinjuku-ku, Tokyo 162-8640, Japan*
[b] *Graduate School of Infection Control Sciences, Kitasato University, Shirokane 5-9-1, Minato-ku, Tokyo 108-8641, Japan*
[c] *Department of Bioactive Molecules, National Institute of Infectious Diseases, 1-23-1, Toyama, Shinjuku-ku, Tokyo 162-8640, Japan*
[d] *Laboratory of Viral Pathogenesis, Institute for Virus Research, Kyoto University, Kyoto 606-8507, Japan*

Received 26 August 2008; revised 10 October 2008; accepted 21 October 2008

Available online 7 November 2008

Edited by Ivan Sadowski

Abstract **We conducted a phenotypic cDNA screening using a T cell line-based assay to identify human genes that render cells resistant to human immunodeficiency virus type 1 (HIV-1). We isolated potential HIV-1 resistance genes, including the carboxy terminal domain (CTD) of bromodomain-containing protein 4 (Brd4). Expression of GFP-Brd4-CTD was tolerated in MT-4 and Jurkat cells in which HIV-1 replication was markedly inhibited. We provide direct experimental data demonstrating that Brd4-CTD serves as a specific inhibitor of HIV-1 replication in T cells. Our method is a powerful tool for the identification of host factors that regulate HIV-1 replication in T cells.**

Keywords: HIV-1 replication; Host factor; cDNA library; Brd4; P-TEFb complex; Tat-dependent LTR transcription

1. Introduction

The identification of specific molecular interactions required for efficient HIV-1 replication should provide clues towards improved understanding of the mechanisms of viral pathogenesis, as well as of host defence against HIV-1. In addition, this may help design highly specific inhibitors against HIV-1. Genome-wide screening for HIV-1 replication regulatory factors has been attempted by using various experimental approaches. Most of them were based on adherent epithelial cells, because these cells exhibit higher transduction efficiencies (by transfection or by viral vector transfer) when compared with T cell lines [1,2]; however, cells of epithelial origin are not relevant hosts for HIV-1 in vivo. Furthermore, viral vectors pseudotyped with vesicular stomatitis virus-G (VSV-G) are often used for screening purposes, instead of wild-type HIV-1. These vectors enter cells via the VSV-G-restricted route, which is different from the HIV-1 envelope-mediated entry pathway. These factors constitute potential caveats of these assays.

To overcome these potential problems, we carried out a phenotypic screen to identify human cDNAs that confer resistance to HIV-1 replication, without affecting cell proliferation. The assay was performed in a human T cell line, a physiologically relevant host, stably transduced with a human cDNA library. We isolated several potential HIV-1 resistance genes successfully, many of which were not known as HIV-1 regulatory factors. In this work, we studied Brd4 in detail to demonstrate the applicability of our phenotype screening. Our study of Brd4-CTD suggests the presence of a potential anti-HIV-1 drug target in the host transcription regulator cyclin T1 (CCNT1).

2. Materials and methods

2.1. Cells and transfection

Cells were maintained in RPMI 1640 medium (Sigma, St. Louis, MA) supplemented with 10% fetal bovine serum (Japan Bioserum, Tokyo), 50 U/ml penicillin, and 50 μg/ml streptomycin (Invitrogen, Tokyo, Japan), and then incubated at 37 °C in a humidified 5% CO_2 atmosphere. Cells were transfected with Lipofectamine 2000 according to the manufacturer's protocol (Invitrogen).

2.2. Plasmid construction

The Brd4-CTD was amplified from 293T RNA by reverse transcriptase PCR (RT-PCR) using the primers 5′-AGATCTCTCATCCGACCACCCCCTCCTCC-3′ and 5′-TCAGGATCCCGAAAAGATTTTCTTCAAATATTG-3′. The BglII–BamHI fragment of the PCR product was cloned into the corresponding restriction sites of the pEGFP-C2 (Clontech, Palo Alto, CA). The XhoI–MfeI fragment from the resulting plasmid was cloned into the corresponding restriction sites of the pCMMP KRAB vector, creating the pGFP-Brd4-CTD. The cDNA encoding firefly luciferase (Luc$^+$) was amplified by PCR from the pGL3-Basic (Promega, Madison, WI) using the primers 5′-ACCGGTCTCGAGGGCCACCATGGAAGACGCCAAAAACATAAAGAAAGG-3′ and 5′-GAATTCGGATCCTTACACGGCGATCTTTCCGCCCTTCTTGGCC-3′. The PCR product was digested with AgeI and BamHI, and cloned into the corresponding sites of the pCMMP GFP vector, generating the pCMMP Luciferase. The BamHI–XhoI fragment of pLenti6/V5-GW/lacZ (Invitrogen) was removed, and Luc$^+$ was inserted with BglII and SalI sites artificially attached at its extremities, creating the pLenti Luciferase. Other plasmids used in this study were described previously [3,4].

*Corresponding author. Fax: +81 3 5285 5037.
E-mail address: ajkomano@nih.go.jp (J. Komano).

0014-5793/$34.00
doi:10.1016/j.febslet.2008.10.047

2.3. Selecting human cDNAs that confer resistance to HIV-1

The lentiviral vector carrying an hPBL cDNA library was described previously [5]. MT-4 cells (1×10^6) transduced with the cDNA library were infected with HIV-1_{HXB2} propagated in MT-2 cells, by resuspending MT-4 cells in a viral preparation containing 70–1250 ng/ml p24 viral capsid antigen in 20 ml of culture medium for 30 min at room temperature with continuous mixing. Anti-CD4 magnetic beads (0.5–1.0×10^7; Dynal, Oslo, Norway) were added to the cell suspension to prevent cell-to-cell contact, and the cells (1×10^3 cells per well in 200 μl of culture medium) were plated in flat-bottomed 96-well plates. At 3–4 weeks post-infection, cells from four wells positive for cell outgrowth were pooled and genomic DNA was extracted. The cDNA inserts were PCR-amplified and sequenced using primers described previously [5].

2.4. Generation of viruses and infection

Viruses were produced as described previously [3,4]. Human T cell lines (MT-4 and Jurkat cells; 1×10^5 cells) were incubated with 500–1000 μl of MLV preparations in the presence of 8 μg/ml polybrene for 1 h at 4 °C with continuous agitation. For HIV-1 infection, 1×10^5 cells were incubated with an HIV-1-containing culture supernatant (*ca.* 5–5000 pg p24), for 30 min at room temperature. HIV-1 replication was monitored as described previously [3,4].

2.5. Western blotting

Western blotting was performed according to techniques described previously [4]. The following antibodies were used: anti-CCNT1 (ab2098, Abcam, MA), anti-Brd4 (ab46199, Abcam), anti-GFP (MAB3580, Chemicon International, Temecula, CA or 632381, Clontech), anti-p24 (183-H12-5C, NIH AIDS Research and Reference Reagent Program), anti-HEXIM1 (ab25388, Abcam), anti-Bip/GRP78 (clone 40, BD Transduction Laboratories), and EnVision+ system (Dako, Glostrup, Denmark).

2.6. Reporter assay

The 293T cells grown in 48-well plates were co-transfected with 20 ng of pLTR-Luc or pCMMP Luciferase, together with pGFP-Brd4-CTD. The total amount of transfected DNA was adjusted by pCMMP GFP. To measure the effect of Tat, cells were co-transfected with 100 ng of pSVtat in addition to the above-mentioned plasmids. Cells were replated in 96-well plates in triplicate at 2–4 h post-transfection. Luciferase activity was measured 48 h after transfection using the Dual-Glo assay kit (Promega).

2.7. RT-PCR

RT-PCR was performed as described previously [4]. For amplification of HIV-1 mRNA, forward (5′-CTCGACGCAGGACTCGGCTTGC-3′) and reverse (5′-AGTTCCACTCCTGCCCAAGTATCC-3′) primers were used. The mRNA encoding glyceraldehyde-3-phosphate dehydrogenase (GAPDH) was amplified using the primers 5′-GTGGAAGGACTCATGACCACAGTC-3′ and 5′- CATGTGGGCCATGAGGTCCACCAC-3′.

2.8. Quantitative real-time PCR

The real-time PCR reaction was performed as described previously [4]. Amplifications were performed using the QuantiTect SYBR Green RT-PCR/PCR Kit (QIAGEN). To estimate the amount of integrated HIV-1 DNA, Alu-LTR PCR was performed as described previously [6] using the following primers: first PCR reaction, 5′-AACTAGGGAACCCACTGCTTAAG-3′ and 5′-TGCTGGGATTACAGGCGTGAG-3′; and second PCR reaction, 5′-AACTAGGGAACCCACTGCTTAAG-3′ and 5′-CTGCTAGAGATTTTCCACACTGAC-3′.

3. Results

To isolate cDNA clones that confer resistance to HIV-1 without negatively affecting cell proliferation, we performed phenotype screening using MT-4 cells stably transduced with a lentiviral vector carrying a cDNA library from human peripheral blood lymphocytes (hPBL). The complexity of the lentiviral cDNA library was on the order of 10^6. The lentiviral vector encoded a GFP expression cassette. Approximately 70% of the MT-4 cells became GFP-positive after infection of the lentiviral vector, suggesting that a portion of the cells were infected with multiple lentiviral vectors. The GFP-positive cells were collected using a FACS sorter and subsequently exposed to replication-competent HIV-1. The surviving cell clones were propagated and their transduced cDNAs were examined. The average length of hPBL cDNA in the lentiviral vector was ~0.7 kbp, which is shorter than the average human cellular mRNA length (~2 kbp). A gene was considered an innate

Table 1
Summary of cDNAs recovered in an HIV-1-resistant phenotype screening in MT-4 cells.

Gene category	# of independent clones	Frequency (%)	Frequently isolated genes[a] (# of independent clones)
Metabolism	16	24.6	Haemoglobin (7) Pyridoxal kinase, PDXK (3)
Transcription	7	10.8	Bromodomain containing 4, Brd4 (3) Zinc finger protein 26, ZNF26 (3)
Ribosomal proteins	7	10.8	Ribosomal protein L14, RPL14 (3)
Signal transduction	7	10.8	Zinc finger protein 36, ZFP36L2 (2) transducin beta-like 1X-linked, TBL1X (1)[c] Chromosome 22 open reading frame 5, C22orf5 (1)[c]
Trafficking	6	9.2	Chromosome 9 open reading frame 86, C9orf86 (1)[b] Chromosome 1 open reading frame 142, C1orf142 (1)[b] Nedd4-binding partner 3, N4BP3 (1)
Immunology	2	3.1	MHC class II, DR alpha (1)
Oncogenesis	2	3.1	AXIN1 up-regulated, AXUD1 (1)[c]
Glycosylation	2	3.1	Hyaluronan and proteoglycan link protein 3, HAPLN3 (1)
Differentiation	2	3.1	Jumonji AT rich interactive domain 2, JARID2 (1)
Cytoskeleton	2	3.1	Beta actin (1)
Cell cycle control	1	1.5	CWF19-like 1, CWF19L1 (1)
Apoptosis	1	1.5	Chromosome 2 open reading frame 28, C2orf28 (1)
DNA repair	1	1.5	Non-SMC element 1 homolog, NSMCE1 (1)[b]
Non-ORF coding	9	13.8	–
Total	65	100.0	–

[a]All the clones isolated more than three times are listed. A representative clone is shown for categories with a few candidates.
[b]These genes exhibited regulatory functions on HIV-1 production.
[c]These genes exhibited no effect on HIV-1 production.

negative factor for HIV-1 replication if the full-length open reading frame (ORF) was recovered. Alternatively, if a portion of a gene was recovered, the full-length gene was considered a potential positive factor for HIV-1 replication. We recovered 65 independent cDNA clones (43 genes, Table 1). A number of cDNAs encoded abundant cellular transcripts, including haemoglobin. In addition, cDNAs encompassing non-ORFs were isolated. The isolation of these cDNAs was likely due to the infection of a single cell with multiple cDNA-transducing lentiviral vectors, one of which encoded an HIV-1 resistance gene. If we disregard these cases, 26 genes were potential HIV-1 regulatory gene candidates, of which seven were examined for a potential HIV-1 regulatory functions as shown in Fig. 2. Four genes exhibited HIV-1 regulatory phenotypes (4/7 genes, 57.1%; Table 1). In addition to Brd4-CTD, C9orf86 and NSMCE1 scored as positive factors for HIV-1 replication, and C1orf142 was scored as a negative factor. This suggested that our screening was successful in selecting for HIV-1 regulatory genes. While each candidate gene will be studied in detail in future studies, here we focused on Brd4.

Brd4 was chosen for three reasons: (1) three independent Brd4 cDNAs were recovered; (2) Brd4 binds to the CCNT1/T2-bearing P-TEFb complex [7,8]; and (3) 13 independent Brd4 cDNA clones (13/42 clones, 31.0%) were isolated from a similar experiment in which the cDNA library from an *Oryctolagus cuniculus* kidney derived cell line was used. All the three Brd4 cDNA clones encoded Brd4-CTD: two encoded amino acids (aa) 1260–1362 and the third encoded aa 1209–1362 (Fig. 1A). The first two clones were translated using the Met-encoding codon at Brd4 nucleotide position 3778–3780, and the third was translated from the aberrant start codon in the primer upstream of the Brd4 ORF 3628 nt. To our surprise, aa fragment 1209–1264 of Brd4 was recently reported as an interactor of CCNT1 that inhibits Tat-dependent LTR-driven transcription [9]; however, the specific effect of this region on HIV-1 replication in human T cells was not fully investigated.

We hypothesized that the repression of HIV-1 replication in MT-4 cells may be due to the selective inhibition of viral gene transcription by Brd4-CTD. To test this, we cloned Brd4-CTD spanning aa 1209-1364 into a retroviral plasmid and fused GFP to its carboxy-terminus (GFP-Brd4-CTD, Fig. 1B). Confocal microscopy revealed that GFP-Brd4-CTD was localized mainly in the cytoplasm of MT-4 cells, with some signal found in the nucleus (Fig. 1C). A transient transfection assay revealed that the expression of GFP-Brd4-CTD modestly enhanced the luciferase expression driven by both the LTR and CMV promoters (Fig. 1D). In the presence of Tat, LTR

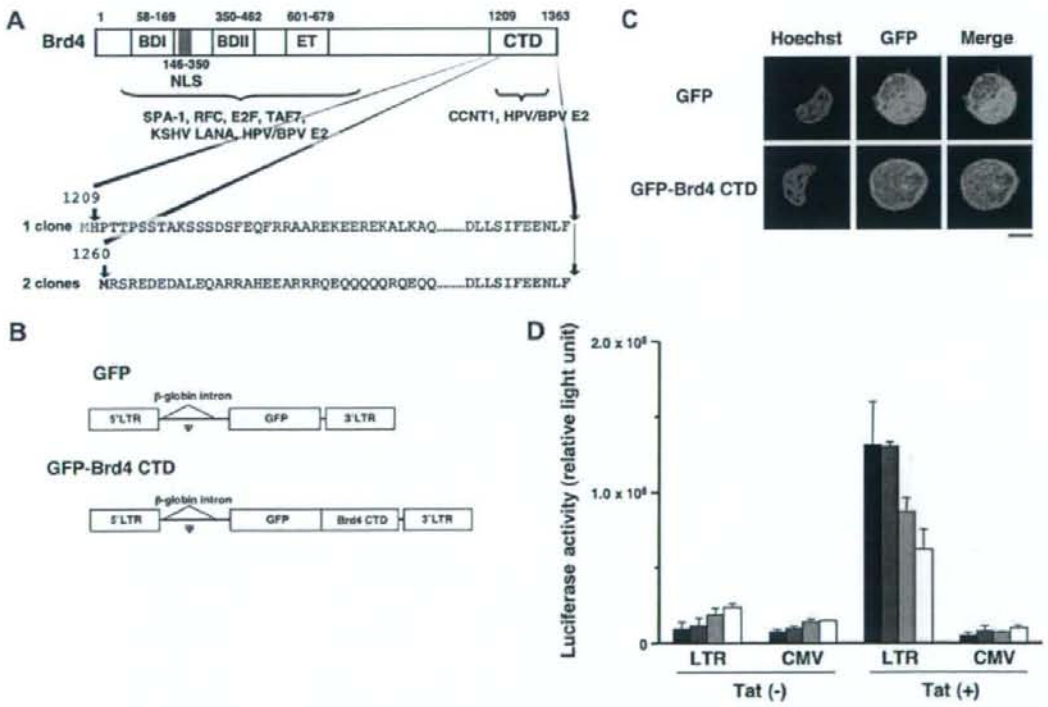

Fig. 1. Specific inhibition of Tat-dependent LTR transcription by GFP-Brd4-CTD. (A) Functional properties of the Brd4 domains and isolated Brd4 cDNAs. (B) Construction of MLV vector-based mammalian expression plasmids encoding GFP or GFP-Brd4-CTD. (C) Confocal microscopy images of MT-4 cells stably expressing GFP or GFP-Brd4-CTD. Green and blue represent GFP and the Hoechst 33258-stained nuclei, respectively. Magnification, 630×; scale bar, 5 μm. (D) Effect of GFP-Brd4-CTD on LTR and CMV promoter activities in the absence or presence of the Tat expression plasmid. Cells transfected with 0, 16, 80, and 400 ng of pGFP-Brd4-CTD correspond to black, dark gray, light gray, and white bars, respectively. Representative data from five independent experiments are shown.

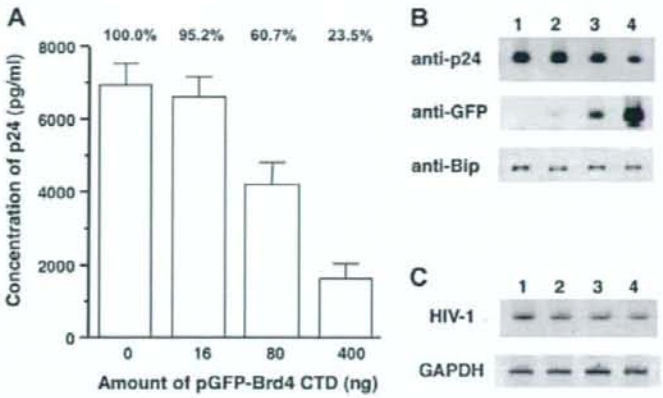

Fig. 2. Inhibition of HIV-1 production by GFP-Brd4-CTD. (A) Viral production was quantified by ELISA detecting p24 viral antigen. The relative decrease in viral levels are indicated on the top of the graph. (B) The viral protein levels in transfected cells were analyzed by Western blotting using the antibodies indicated. (C) The viral spliced transcript and GAPDH mRNA were amplified by RT-PCR. Lanes 1–4 in B and C correspond to the amount of pGFP-Brd4-CTD (0, 16, 80, and 400 ng, respectively). Quantification of these data is summarized in Table 2.

activity was markedly enhanced. When the GFP-Brd4-CTD expression vector was co-transfected, the Tat-dependent enhancement of LTR promoter-driven luciferase expression decreased. A similar trend was not observed for the CMV promoter. These data suggest that the Brd4-CTD specifically limits Tat-dependent LTR transcription.

We also investigated the effect of GFP-Brd4-CTD expression on HIV-1 production by using a proviral DNA mimicking the late phase of the viral life cycle. Consistent with the results described above, transfection of HIV-1 proviral DNA together with an increasing amount of the GFP-Brd4-CTD expression vector led to a decrease of viral yield, as well as of the levels of viral protein and mRNA in the transfected cells (Fig. 2). The viral RNA levels dropped in parallel with the protein levels, as demonstrated by real-time RT-PCR analysis (Fig. 2C and Table 2). These data suggest that GFP-Brd4-CTD inhibits HIV-1 production by blocking viral transcription.

To confirm the blockage of HIV-1 replication by Brd4-CTD, GFP-Brd4-CTD was transduced into MT-4 and Jurkat cells using an MLV-based vector (Fig. 3A). Green fluorescence indicated that the efficiency of MLV-mediated gene transduction in MT-4 cells was >90%, with a lower transduction efficiency observed in Jurkat cells, as estimated by FACS analysis. The GFP-positive Jurkat cells were collected using a FACS sorter. The expression of GFP and GFP-Brd4-CTD was verified by Western blot analysis (Fig. 3B). The expression levels of transcription-related gene products were not detectably affected by the constitutive expression of GFP-Brd4-CTD (Fig. 3B). In addition, there was no detectable difference in the levels of cell-surface HIV-1 receptors (CD4 and CXCR4), cell morphology, and cell proliferation rates between GFP- and GFP-Brd4-CTD-expressing cells (Fig. 1C and Supplementary data). We found that HIV-1 replicated less efficiently in GFP-Brd4-CTD-expressing cells than in GFP-expressing cells, in both cell lines tested, which confirms the HIV-1-resistant phenotype of MT-4 cells (Fig. 3C). The efficiency of viral genome integration into GFP-Brd4-CTD-expressing cells was indistinguishable from that of GFP-expressing cells (103.2 ± 24.1%) as examined by Alu-LTR PCR, suggesting that the early phase of the viral life cycle was not blocked by GFP-Brd4-CTD.

4. Discussion

Our phenotype screening method proved to be a powerful tool because a human T cell line was subjected to HIV-1 resistance screening by stable and non-transient introduction of a human cDNA library, and because wild-type HIV-1 was used; thus, the effect of candidate gene expression on cell proliferation was less of a concern in this system when compared with transient assay systems. In addition, HIV-1 inhibitory genes were isolated at a frequency of ~15% (4/26 genes), 75% of which were novel. We therefore believe that our system is remarkable in selecting genes that confer HIV-1 resistance in T cells. By applying this assay to other cDNA libraries, we

Table 2
Effect of GFP-Brd4-CTD on viral production examined by quantitative real time RT-PCR and ELISA.

pGFP-Brd4-CTD (ng)	HIV-1 mRNA (copy)[a]	GAPDH mRNA (copy)[a]	Ratio (HIV-1/GAPDH)	Normalized (%)[b]	p24 ELISA (%)[c]
0	274250	261750	1.048	100.0	100.0
16	221600	228850	0.968	92.4	95.2
80	138050	311450	0.443	42.3	60.7
400	120850	347750	0.348	33.2	23.5

[a]Copy per 100 ng total cellular RNA.
[b]Relative reduction of HIV-1 mRNA considering pGFP-Brd4-CTD 0 ng as 100%.
[c]See Fig. 2.

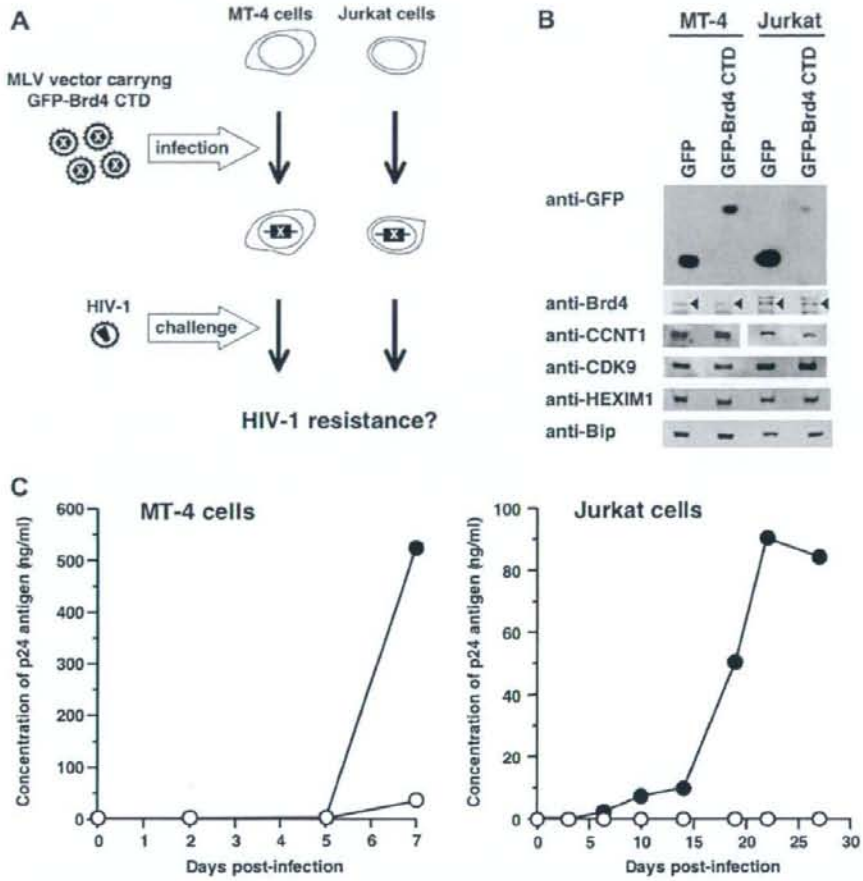

Fig. 3. Constitutive expression of GFP-Brd4-CTD limited the replication of HIV-1. (A) Experimental design. MT-4 and Jurkat cells were transduced with an MLV vector expressing GFP-Brd4-CTD. Cells were challenged by HIV-1 and the efficiency of viral replication was examined. (B) Western blot analysis of the expression levels of GFP, GFP-Brd4-CTD, Brd4 (arrowhead), CCNT1, CDK9, HEXIM1, and BiP in established MT-4 and Jurkat cells. (C) HIV-1 replication kinetics in MT-4 and Jurkat cells constitutively expressing GFP (black circles) or GFP-Brd4-CTD (white circles). Representative data from two independent experiments are shown.

may be able to isolate novel cellular factors that regulate HIV-1 replication.

The assessment of the selective impact of altered candidate gene expression or function on HIV-1 replication (without the alteration of cell proliferation) is critical to the identification of cellular molecular targets for novel anti-retroviral drugs. We demonstrated that Brd4-CTD was a specific silencer of HIV-1 replication, and verified that it effectively blocked HIV-1 replication in multiple human T cell lines without affecting cell proliferation. Our data indicate that primate lentiviral replication is more heavily dependent on the CCNT1-containing P-TEFb complex than cellular gene transcription, which is consistent with previous findings [4,10–11]. This implies that HIV-1 replication can be controlled by selectively restricting the CCNT1-containing P-TEFb complex. Our transcription assay indicated that the Brd4-CTD is not an inhibitor of the P-TEFb complex, but is rather a functional Tat inhibitor. Previous biochemical studies have suggested that Brd4-CTD and Tat bind to CCNT1 in a reciprocally exclusive fashion [7,9]. Given that the binding regions of these two proteins do not overlap, Brd4-CTD may be an allosteric inhibitor of the Tat-CCNT1 interaction. Taken together, our results indicate that the Brd4-interacting region of CCNT1 is a potential molecular target for the development of a novel HIV-1 inhibitor.

Acknowledgements: This work was supported by the Japan Health Science Foundation, the Japanese Ministry of Health, Labor and Welfare (H18-AIDS-W-003) and the Japanese Ministry of Education, Culture, Sports, Science and Technology (18689014 and 18659136).

Appendix A. Supplementary data

Supplementary data associated with this article can be found, in the online version, at doi:10.1016/j.febslet.2008.10.047.

References

[1] Valente, S.T. and Goff, S.P. (2006) Inhibition of HIV-1 gene expression by a fragment of hnRNP U. Mol. Cell 23, 597–605.

[2] Brass, A.L., Dykxhoorn, D.M., Benita, Y., Yan, N., Engelman, A., Xavier, R.J., Lieberman, J. and Elledge, S.J. (2008) Identification of host proteins required for HIV infection through a functional genomic screen. Science 319, 921–926.

[3] Komano, J., Miyauchi, K., Matsuda, Z. and Yamamoto, N. (2004) Inhibiting the Arp2/3 complex limits infection of both intracellular mature vaccinia virus and primate lentiviruses. Mol. Biol. Cell 15, 5197–5207.

[4] Shimizu, S. et al. (2007) Inhibiting lentiviral replication by HEXIM1, a cellular negative regulator of the CDK9/cyclin T complex. AIDS 21, 575–582.

[5] Kawano, Y., Yoshida, T., Hieda, K., Aoki, J., Miyoshi, H. and Koyanagi, Y. (2004) A lentiviral cDNA library employing lambda recombination used to clone an inhibitor of human immunodeficiency virus type 1-induced cell death. J. Virol. 78, 11352–11359.

[6] Biglione, S., Byers, S.A., Price, J.P., Nguyen, V.T., Bensaude, O., Price, D.H. and Maury, W. (2007) Inhibition of HIV-1 replication by P-TEFb inhibitors DRB, seliciclib and flavopiridol correlates with release of free P-TEFb from the large, inactive form of the complex. Retrovirology 4, 47.

[7] Jang, M., Mochizuki, K., Zhou, M., Jeong, H., Brady, J. and Ozato, K. (2005) The bromodomain protein Brd4 is a positive regulatory component of P-TEFb and stimulates RNA polymerase II-dependent transcription. Mol. Cell 19, 523–534.

[8] Yang, Z., Yik, J., Chen, R., He, N., Jang, M., Ozato, K. and Zhou, Q. (2005) Recruitment of P-TEFb for stimulation of transcriptional elongation by the bromodomain protein Brd4. Mol. Cell 19, 535–545.

[9] Bisgrove, D.A., Mahmoudi, T., Henklein, P. and Verdin, E. (2007) Conserved P-TEFb-interacting domain of BRD4 inhibits HIV transcription. Proc. Natl. Acad. Sci. USA 104, 13690–13695.

[10] Urano, E. et al. (2008) Cyclin K/CPR4 inhibits primate lentiviral replication by inactivating Tat/positive transcription elongation factor b-dependent long terminal repeat transcription. AIDS 22, 1081–1083.

[11] Salerno, D., Hasham, M.G., Marshall, R., Garriga, J., Tsygankov, A.Y. and Grana, X. (2007) Direct inhibition of CDK9 blocks HIV-1 replication without preventing T-cell activation in primary human peripheral blood lymphocytes. Gene 405, 65–78.

Journal of General Virology (2008), 89, 3144–3149 DOI 10.1099/vir.0.2008/004820-0

Short Communication

Substitution of the myristoylation signal of human immunodeficiency virus type 1 $Pr55^{Gag}$ with the phospholipase C-δ1 pleckstrin homology domain results in infectious pseudovirion production

Emiko Urano,[1,2] Toru Aoki,[1] Yuko Futahashi,[1] Tsutomu Murakami,[1] Yuko Morikawa,[2] Naoki Yamamoto[1] and Jun Komano[1]

Correspondence
Jun Komano
ajkomano@nih.go.jp

[1]AIDS Research Center, National Institute of Infectious Diseases, 1-23-1 Toyama, Shinjuku-ku, Tokyo 162-8640, Japan

[2]Kitasato Institute of Life Sciences, Kitasato University, Shirokane 5-9-1, Minato-ku, Tokyo 108-8641, Japan

The matrix domain (MA) of human immunodeficiency virus type 1 $Pr55^{Gag}$ is covalently modified with a myristoyl group that mediates efficient viral production. However, the role of myristoylation, particularly in the viral entry process, remains uninvestigated. This study replaced the myristoylation signal of MA with a well-studied phosphatidylinositol 4,5-biphosphate-binding plasma membrane (PM) targeting motif, the phospholipase C-δ1 pleckstrin homology (PH) domain. PH–Gag–Pol PM targeting and viral production efficiencies were improved compared with Gag–Pol, consistent with the estimated increases in Gag–PM affinity. Both virions were recovered in similar sucrose density-gradient fractions and had similar mature virion morphologies. Importantly, PH–Gag–Pol and Gag–Pol pseudovirions had almost identical infectivity, suggesting a dispensable role for myristoylation in the virus life cycle. PH–Gag–Pol might be useful in separating the myristoylation-dependent processes from the myristoylation-independent processes. This the first report demonstrating infectious pseudovirion production without myristoylated $Pr55^{Gag}$.

Received 11 June 2008
Accepted 20 August 2008

The N-terminal region [$p17^{MA}$, matrix (MA) domain] of human immunodeficiency virus type 1 (HIV-1) $Pr55^{Gag}$ (Gag), a structural protein with multiple roles in the virus life cycle (Swanstrom & Wills, 1997), is covalently modified with a myristyol group that aids in plasma membrane (PM) targeting. Removal of this region leads to inefficient Gag targeting to the PM, resulting in dramatically reduced virus production (Bryant & Ratner, 1990; Göttlinger *et al.*, 1989; Pal *et al.*, 1990; Zhou *et al.*, 1994). Although viral particles can be produced by substituting MA with heterologous PM-targeting motifs, such substitution mutants show markedly reduced infectivity (Jouvenet *et al.*, 2006; Scholz *et al.*, 2008), probably due to an active role of MA in viral entry (Kiernan *et al.*, 1998; Wang *et al.*, 1993). However, direct experimental evidence of a viral entry-specific role for MA myristoylation is lacking. Such specific roles of Gag myristoylation can only be determined by separating the myristoylation-dependent PM-targeting function from other MA-associated functions.

We constructed a mutant *gag* expression plasmid where the myristoylated region of Gag was replaced with the N-terminal pleckstrin homology (PH) domain of phospholipase C-δ1 (PLCδ1), a well-studied cellular PM-targeting motif that functions similarly to the myristoyl moiety. PLCδ1 is a member of a family of inositol phospholipid-specific PLC isozymes involved in transducer-mediated intracellular responses (Berridge, 1993). The ~120 aa PH domain can bind to phosphatidylinositol 4,5-biphosphate [PI(4,5)P(2)] and localize to the PM with high affinity and specificity (Ferguson *et al.*, 1995b; Fiorentini *et al.*, 2006; Harlan *et al.*, 1994, 1995; Rhee, 2001; Yagisawa *et al.*, 1994), and green fluorescent protein-bound PLCδ1 PH domains have been used to visualize the PM in living cells (Stauffer *et al.*, 1998; Tall *et al.*, 2000).

We used a codon-optimized HIV-1 *gag–pol* expression vector (p*gag–pol*) for genetic modification of *gag*, as p*gag–pol* increases Gag expression and facilitates protein analyses (Wagner *et al.*, 2000). The substituted mutant retained an intact MA, with the exception of two N-terminal amino acid mutations (ATG→CTG and GGC→GCG), resulting in an MG→LA mutation to knock out the myristoylation signal of Gag and prevent internal translational initiation (Fig. 1a). The PLCδ1 PH domain residues 1–175 (Stauffer *et al.*, 1998) were linked to the LA–Gag N terminus by the amino acids PRAEFT, creating a PH–*gag–pol* expression vector (pPH-*gag-pol*, Fig. 1a). A control PH domain

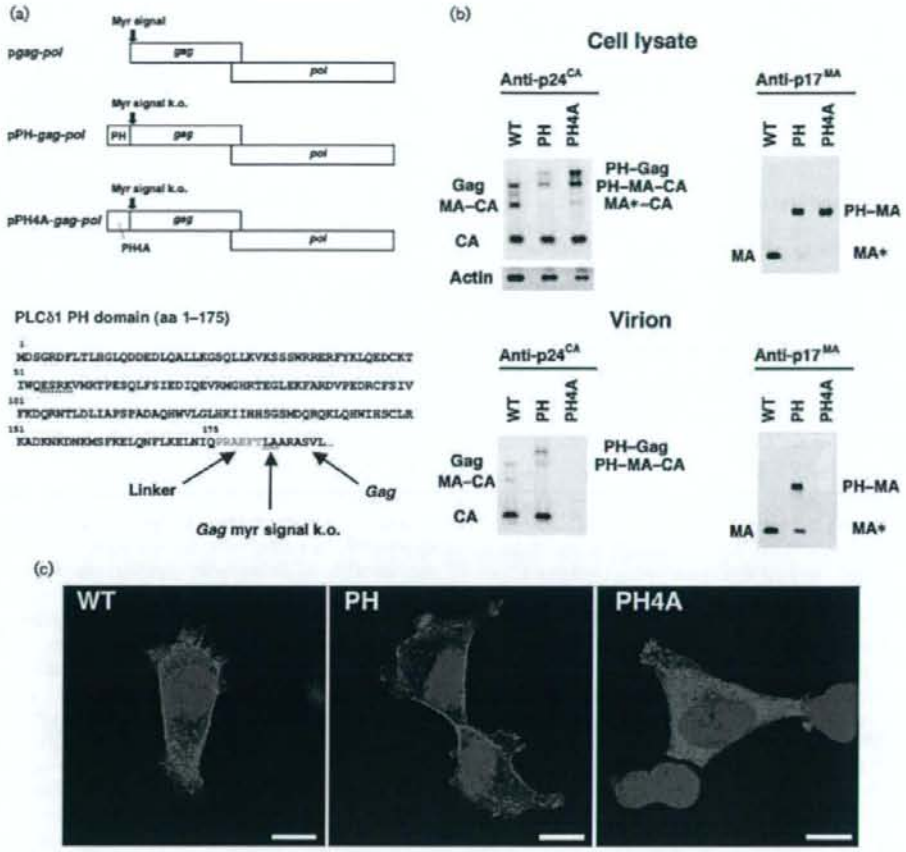

Fig. 1. Viral production by the *gag–pol* expression vectors. (a) The genetic structure of the p*gag-pol*, pPH-*gag-pol* and pPH4A-*gag-pol* expression vectors, and the amino acid sequence of the PH–Gag junction are shown. The N-terminal PH domain of PLCδ1 (aa 1–175) was fused to LA–Gag, linked by a 5 aa spacer (shown in grey). The MG→LA mutation to knock out the myristoylation signal of Gag (myr signal k.o.) is underlined. Four alanine mutations were introduced to replace the ESRK sequence (dotted line) to create the PH4A mutant. (b) Protein expression from p*gag-pol* (WT), pPH-*gag-pol* (PH) and pPH4A-*gag-pol* (PH4A) in transfected 293T cell lysates and Gag cleavage in the virions were examined by Western blot analysis using anti-$p24^{CA}$ or anti-$p17^{MA}$ antibodies. Note that the anti-$p17^{MA}$ antibody recognizes the cleaved $p17^{MA}$ protein only. The band denoted as PH–MA–CA in the virion detected by the anti-$p24^{CA}$ antibody (lower left panel) possibly overlaps with a faint Gag signal derived from PH–Gag and PH4A–Gag from which the PH and PH4A domains have been cleaved. (c) Immunofluorescence assay showing the distribution of Gag, PH–Gag and PH4A–Gag in 293T cells transfected with the respective expression plasmid. Red and blue represent $p24^{CA}$ and the Hoechst 33258-stained nucleus, respectively. Bars, 10 μm.

mutant (PH4A) had mutations at aa 54–57 (ESRK→AAAA; Fig. 1a); these residues are responsible for the PH domain–PI(4,5)P(2) interaction (Ferguson *et al.*, 1995a). PH–Gag, PH4A–Gag and their cleaved products were detected in transfected 293T cell lysates with mouse monoclonal antibodies specific for the $p24^{CA}$ (capsid) domain (anti-$p24^{CA}$; NIH AIDS Research and Reference Reagent Program) and MA domain (anti-$p17^{MA}$; Advanced Biotechnologies) (Fig. 1b). PH–Gag cleavage was more efficient than that of Gag, suggesting efficient PM targeting of PH–Gag (Fig. 1b). The Gag protein levels in the pPH4A-*gag-pol*-transfected cell lysate were higher than those in p*gag-pol*- and pPH-*gag-pol*-transfected cell lysates when adjusted for the amount of protein loaded, indicating the low virus-like particle (VLP) production efficiency by PH4A–Gag (Fig. 1b).

The intracellular distribution of Gag, PH–Gag and PH4A–Gag was analysed by immunofluorescence microscopy of transfected 293T cells (Fig. 1c). Transfected cells were grown for 24 h, fixed (4 % formaldehyde), permeabilized (0.1 % Triton X-100 for 5–30 min) and incubated with mouse anti-$p24^{CA}$ and goat anti-mouse antibodies (GE Healthcare Bio-Sciences) conjugated to streptavidin–Alexa Fluor 555 (Invitrogen). Cells were stained with Hoechst 33258, mounted and analysed using confocal microscopy as described previously (Futahashi *et al.*, 2007). Gag was found to be distributed throughout the cytoplasm and at the cell periphery. In contrast, PH–Gag signals were mostly detected at the cell periphery and PH4A–Gag was distributed homogeneously in the cytoplasm. These data clearly showed that PH–Gag targeted the PM more efficiently than Gag, consistent with the Western blot analysis (Fig. 1b). These results also suggested that the efficient PM targeting of PH–Gag depends on the ability of the PH domain to bind PI(4,5)P(2). Similar observations were made in NP2 and COS7 cells.

VLP production was also examined. Tissue culture supernatants of p*gag-pol*-, pPH-*gag-pol*- or pPH4A-*gag-pol*-transfected 293T cells were passed through nitrocellulose filters (0.45 μm) and the virions were collected by centrifugation (541 000 ***g*** for 1 h). Viral antigens, except for PH4A, were detected with anti-$p24^{CA}$ and anti-$p17^{MA}$ antibodies (Fig. 1b). Gag and PH–Gag were further processed by the viral proteases in the virions compared with the cell lysates, as indicated by the increased signals for CA and MA relative to Gag. Interestingly, approximately one-fifth of the PH–Gag in the virion was cleaved close to the PH–MA junction. Presumably, the amino acid sequence at the C end of the PH domain ELQN/FLKE (aa 164–171, where the protease cleaves at the N–F junction) served as a viral protease recognition site as it matched the substrate consensus sequence and resembled the NC–*p1* junction, RQAN/FLGK (de Oliveira *et al.*, 2003; Swanstrom & Wills, 1997). Alternatively, the N terminus of LA–Gag (EFTL/AADS) might be targeted by the viral protease. Thus, the MA released from PH–MA, designated MA*, possibly has 10 aa attached to its N terminus.

The VLP production efficiency was quantified as the concentration of CA in transfected 293T cell culture supernatants relative to that in cell lysates using a p24 ELISA (Zeptometrics). When the CA concentrations of the virion fractions were normalized to those of the cell lysates, the pPH-*gag-pol* viral production efficiency was 3.2-fold higher than that of p*gag-pol* (3.2 ± 2.0-fold, $n=14$, $P<0.001$ by Wilcoxon's matched pairs rank test; representative experiments are shown in Table 1). In contrast, pPH4A-*gag-pol* produced viral particles less efficiently than p*gag-pol* (0.09 ± 0.07-fold, $n=6$, $P<0.05$ by Wilcoxon's matched pairs rank test; representative experiments are shown in Table 1). These data were consistent with the Western blot analysis (Fig. 1b).

To characterize the physical properties of PH–Gag–Pol VLPs, we measured the specific density of virions and examined the virion morphology. Firstly, the VLPs were subjected to 20–70 % (w/w) equilibrium sucrose gradient centrifugation (120 000 ***g*** for 16 h) and fractions were recovered from the bottom to the top. The peak fraction containing the viral CA antigen was determined by p24 ELISA. Gag–Pol and PH–Gag–Pol VLPs were detected in fractions with densities of 1.15 ± 0.01 ($n=5$) and 1.16 ± 0.01 ($n=4$) g ml^{-1}, respectively (not statistically significant; representative experiments are shown in Fig. 2a). Secondly, ultrathin sections of fixed 293T cells (2 % glutaraldehyde, 2 % osmium tetroxide) transfected with p*gag-pol* or pPH-*gag-pol* were imaged by transmission electron microscopy (JEM1200EX at 80 kV or JEM2000EX at 100 kV; JEOL). The PH–Gag–Pol and Gag–Pol VLP

Table 1. Efficiency of virus production from 293T cells transfected with p*gag-pol*, pPH-*gag-pol* or pPH4A-*gag-pol* expression vector

Experiment	Plasmid	$p24^{CA}$ (ng per well)*		Virus production efficiency (B/A)	Fold increase relative to p*gag-pol*
		Cell lysate (A)	Culture supernatant (B)		
1	p*gag-pol*	4 043	4 869	1.204	–
	pPH-*gag-pol*	1 989	8 363	4.206	3.49
	pPH4A-*gag-pol*	3 175	103	0.033	0.03
2	p*gag-pol*	3 521	3 887	1.104	–
	pPH-*gag-pol*	2 638	7 688	2.914	2.64
	pPH4A-*gag-pol*	5 913	1 125	0.190	0.17
3	p*gag-pol*	3 359	4 160	1.239	–
	pPH-*gag-pol*	1 454	5 172	3.558	2.87
	pPH4A-*gag-pol*	4 226	75	0.018	0.01
4	p*gag-pol*	9 666	8 996	0.931	–
	pPH-*gag-pol*	4 699	18 273	3.889	4.18
	pPH4A-*gag-pol*	5 527	534	0.097	0.10

*Cells grown in six-well plates were transfected using Lipofectamine 2000 according to the manufacturer's protocol (Invitrogen).

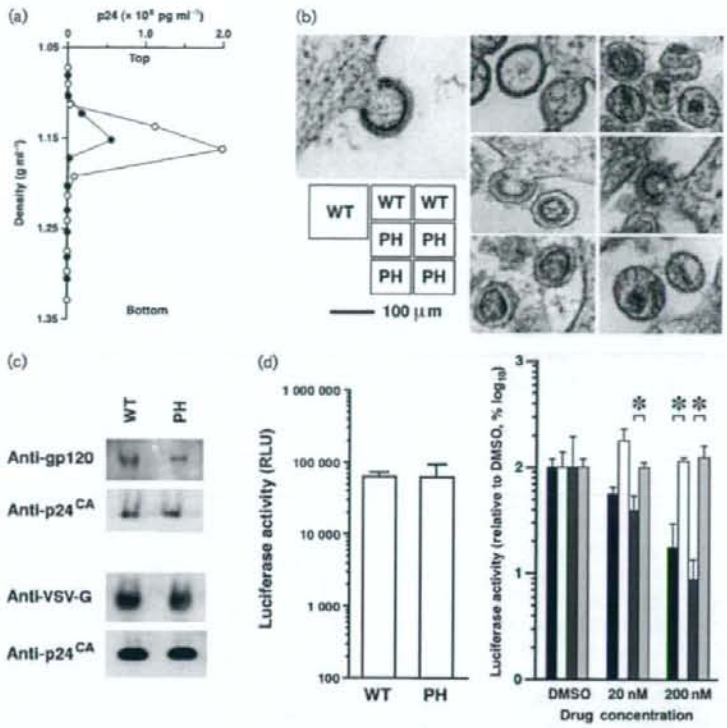

Fig. 2. Physical and biological properties of PH–Gag–Pol VLPs. (a) The virions produced by the *pgag-pol* (WT) and pPH-*gag-pol* (PH) expression vectors were analysed by equilibrium sucrose density-gradient centrifugation. The virion-containing fraction was determined by an ELISA detecting $p24^{CA}$. Representative data from four to five independent experiments are shown. In this experiment, WT (filled circles) and PH (open circles) VLPs migrated in the 1.152 or 1.162 g ml^{-1} density fractions, respectively. (b) Transmission electron microscopy images of 293T cells transfected with *pgag-pol* (WT) or pPH-*gag-pol* (PH). Representative images are shown. (c) Incorporation of HIV-1 Env (upper panel) and VSV-G (lower panel) into Gag–Pol (WT) and PH–Gag–Pol (PH) virions. The virion fractions were subjected to Western blot analysis detecting gp120, VSV-G and $p24^{CA}$. (d) The early phase of the HIV-1 life cycle is supported by PH–Gag–Pol. 293T cells were exposed to virus-containing culture supernatants with similar CA concentrations (270 and 220 ng ml^{-1} for Gag–Pol and PH–Gag–Pol, respectively), and luciferase activities were measured at 2–3 days post-infection as relative light units (RLU). The luciferase activities of PH–Gag–Pol (PH) and Gag–Pol (WT) virus-infected cells were almost identical (left graph). The luciferase transduction by WT (bars 1 and 2) and PH (bars 3 and 4) pseudovirions was performed in the presence of nevirapine (NVP, bars 1 and 3) or TAK-779 (bars 2 and 4). The luciferase signals decreased in the presence of NVP for both WT (bar 1) and PH (bar 3) but not in the presence of TAK-779 for both WT (bar 2) and PH (bar 4), respectively. Representative data from several independent experiments are shown. Asterisks indicate statistical significance ($P<0.01$, $n=3$, Student's *t*-test).

diameters were almost identical (Fig. 2b). Virion budding structures showed that the electron-dense layer, which represented multimerized Gag, of the PH–Gag–Pol VLP was slightly separated from the viral envelope compared with that of the Gag–Pol VLP (Fig. 2b). This indicated that the PH domain was positioned between the viral envelope and the electron-dense layer. In contrast, the morphologies of the mature PH–Gag–Pol and Gag–Pol virions were similar, suggesting that myristoylation is dispensable for mature virion morphology and that the PH–Gag–Pol virion may be infectious.

We examined HIV-1 Env incorporation into the PH–Gag–Pol virion. To do this, we used codon-optimized gp160 (p96ZM651gp160-opt; NIH AIDS Research and Reference Reagent Program). The PH–Gag–Pol virion incorporated HIV-1 Env less efficiently than the Gag–Pol virion as demonstrated by Western blot analysis detecting CA and

gp120 (anti-gp120 antibodies from Santa Cruz Biotechnology; Fig. 2c). This was presumably because PH interfered with the MA–Env interaction. Alternatively, PH may actively incorporate cellular proteins that block efficient Env incorporation into virions. We were unable to evaluate the entry efficacy of PH–Gag–Pol virions pseudotyped by HIV-1 Env because of the limit of detection. PH–Gag–Pol virion infectivity was re-examined by virions pseudotyped with vesicular stomatitis virus G glycoprotein (VSV-G). The incorporation efficiencies of VSV-G into Gag–Pol and PH–Gag–Pol virions were similar (anti-VSV-G antibody from Sigma; Fig. 2c). The lentiviral vector system was used to test this, as HIV-1 provirus gene modifications often fail to produce infectious virions, probably due to viral gene dysregulation. 293T cells were transfected with expression plasmids for Gag–Pol, VSV-G (Komano *et al.*, 2004), Rev and Vpu (a generous gift from Dr H. Göttlinger, University of Massachusetts Medical School, MA, USA), and with a packaging vector encoding a luciferase expression cassette. The HIV-1-based vector expressing firefly luciferase upon infection was recovered 2 days post-transfection. 293T cells were exposed to virus-containing culture supernatants with similar CA concentrations, and luciferase activities were measured at 2–3 days post-infection. When viral preparations with similar p24 concentrations were used, the luciferase activities of PH–Gag–Pol and Gag–Pol virus-infected cells were almost identical to each other (Fig. 2d, left graph). Luciferase expression was blocked by the non-nucleoside reverse transcriptase inhibitor nevirapine (NVP; Boehringer Ingelheim) but not by the CCR5 inhibitor (TAK-779; NIH AIDS Research and Reference Reagent Program), suggesting that gene transduction was mediated by viral infection (Fig. 2d, right panel). Similar results were obtained in several independent experiments. Thus, the PLCδ1 PH domain can functionally replace the HIV-1 Gag myristoylation signal to support both viral production and entry processes, and this myristoylation is dispensable for MA function in the early phase of the virus life cycle. This is the first report describing an infectious pseudovirion without myristoylated Gag. Given that PH–Gag can enhance virus production, HIV-1 with PH–Gag might have been expected to be selected in nature. This is not the case, presumably because the addition of PH to the HIV-1 genome would increase its genome size close to the upper limit that can be incorporated into the retroviral particle, leading to a decrease in genome uptake efficiency, which is clearly a growth disadvantage, despite the enhanced virus production with PH-Gag. More importantly, PH–Gag is unable to incorporate HIV-1 Env efficiently enough to support the production of fully infectious virions. Our data point to the selective advantage of myristoylated Gag in viral evolution.

The myristoylation-dependent Gag–PM association [maximal dissociation constant (K_d) of ~0.5–1.0 $\times 10^{-5}$ M] is presumably important for Gag multimerization at the PM (Provitera *et al.*, 2006). After the first contact of Gag with the PM, the membrane binding of Gag is assumed to be stabilized by the Gag–PI(4,5)P(2) interaction (Ono *et al.*, 2004; Saad *et al.*, 2006). The multimerization of Gag appears to induce a conformational change in MA to expose myristoyl groups to enhance the PM targeting of Gag. The higher-order Gag multimerization is probably facilitated by the increased local concentrations of Gag at the PM. Although Gag and PH–Gag are similar to the extent that PI(4,5)P(2) is involved in their PM association, Gag binds to one of the acyl chains of PI(4,5)P(2), as modelled previously (Saad *et al.*, 2006), whilst the PH domain binds the phosphorylated inositol group (Lemmon *et al.*, 1995). The K_d of binding between the PLCδ1 PH domain and PI(4,5)P(2) (~1–2 $\times 10^{-6}$ M; Lemmon *et al.*, 1995) suggests that the primary force driving PH–Gag to the PM is at least 2.5-fold stronger than that of myristoylation-mediated PM targeting of Gag. This might be one reason why PH–Gag–Pol was 3.2-fold more efficient at virion production than Gag–Pol. Our data suggest that the myristoyl group-dependent Gag–PM affinity is not a prerequisite for efficient Gag assembly at the PM or for viral production.

The MA has multiple functions throughout the virus life cycle (reviewed by Bukrinskaya, 2007; Fiorentini *et al.*, 2006; Hearps & Jans, 2007; Klein *et al.*, 2007). In the PH–Gag–Pol virion, approximately one-fifth of the PH–MA was unanchored from the PM as MA* (Fig. 1b), which might accompany the pre-integration complex to support nuclear targeting. Using PH–Gag–Pol might enable separation of myristoylation-dependent and -independent MA functions, particularly during the entry phase. PH–Gag–Pol might also be useful for producing high-titre lentiviral vectors or for studying Gag trafficking in cells that poorly support PM targeting of myristoylated Gag, such as rodent cells. Furthermore, functional assays comparing the virus production of Gag–Pol and PH–Gag–Pol might enable the identification of chemical inhibitors or cellular factors specifically targeting myristoylated Gag.

Acknowledgements

We thank Dr H. Göttlinger for critically reading the manuscript. This work was supported by the Japan Health Science Foundation, the Japanese Ministry of Health, Labor and Welfare (H18-AIDS-W-003) and the Japanese Ministry of Education, Culture, Sports, Science and Technology (18689014 and 18659136).

References

Berridge, M. J. (1993). Inositol trisphosphate and calcium signalling. *Nature* **361**, 315–325.

Bryant, M. & Ratner, L. (1990). Myristoylation-dependent replication and assembly of human immunodeficiency virus 1. *Proc Natl Acad Sci U S A* **87**, 523–527.

Bukrinskaya, A. (2007). HIV-1 matrix protein: a mysterious regulator of the viral life cycle. *Virus Res* **124**, 1–11.

de Oliveira, T., Engelbrecht, S., Janse van Rensburg, E., Gordon, M., Bishop, K., zur Megede, J., Barnett, S. W. & Cassol, S. (2003). Variability at human immunodeficiency virus type 1 subtype C protease cleavage sites: an indication of viral fitness? *J Virol* **77**, 9422–9430.

Ferguson, K. M., Lemmon, M. A., Schlessinger, J. & Sigler, P. B. (1995a). Structure of the high affinity complex of inositol trisphosphate with a phospholipase C pleckstrin homology domain. *Cell* **83**, 1037–1046.

Ferguson, K. M., Lemmon, M. A., Sigler, P. B. & Schlessinger, J. (1995b). Scratching the surface with the PH domain. *Nat Struct Biol* **2**, 715–718.

Fiorentini, S., Marini, E., Caracciolo, S. & Caruso, A. (2006). Functions of the HIV-1 matrix protein p17. *New Microbiol* **29**, 1–10.

Futahashi, Y., Komano, J., Urano, E., Aoki, T., Hamatake, M., Miyauchi, K., Yoshida, T., Koyanagi, Y., Matsuda, Z. & Yamamoto, N. (2007). Separate elements are required for ligand-dependent and -independent internalization of metastatic potentiator CXCR4. *Cancer Sci* **98**, 373–379.

Göttlinger, H. G., Sodroski, J. G. & Haseltine, W. A. (1989). Role of capsid precursor processing and myristoylation in morphogenesis and infectivity of human immunodeficiency virus type 1. *Proc Natl Acad Sci U S A* **86**, 5781–5785.

Harlan, J. E., Hajduk, P. J., Yoon, H. S. & Fesik, S. W. (1994). Pleckstrin homology domains bind to phosphatidylinositol-4,5-bisphosphate. *Nature* **371**, 168–170.

Harlan, J. E., Yoon, H. S., Hajduk, P. J. & Fesik, S. W. (1995). Structural characterization of the interaction between a pleckstrin homology domain and phosphatidylinositol 4,5-bisphosphate. *Biochemistry* **34**, 9859–9864.

Hearps, A. C. & Jans, D. A. (2007). Regulating the functions of the HIV-1 matrix protein. *AIDS Res Hum Retroviruses* **23**, 341–346.

Jouvenet, N., Neil, S. J., Bess, C., Johnson, M. C., Virgen, C. A., Simon, S. M. & Bieniasz, P. D. (2006). Plasma membrane is the site of productive HIV-1 particle assembly. *PLoS Biol* **4**, e435.

Kiernan, R. E., Ono, A., Englund, G. & Freed, E. O. (1998). Role of matrix in an early postentry step in the human immunodeficiency virus type 1 life cycle. *J Virol* **72**, 4116–4126.

Klein, K. C., Reed, J. C. & Lingappa, J. R. (2007). Intracellular destinies: degradation, targeting, assembly, and endocytosis of HIV Gag. *AIDS Rev* **9**, 150–161.

Komano, J., Miyauchi, K., Matsuda, Z. & Yamamoto, N. (2004). Inhibiting the Arp2/3 complex limits infection of both intracellular mature vaccinia virus and primate lentiviruses. *Mol Biol Cell* **15**, 5197–5207.

Lemmon, M. A., Ferguson, K. M., O'Brien, R., Sigler, P. B. & Schlessinger, J. (1995). Specific and high-affinity binding of inositol phosphates to an isolated pleckstrin homology domain. *Proc Natl Acad Sci U S A* **92**, 10472–10476.

Ono, A., Ablan, S. D., Lockett, S. J., Nagashima, K. & Freed, E. O. (2004). Phosphatidylinositol (4,5) bisphosphate regulates HIV-1 Gag targeting to the plasma membrane. *Proc Natl Acad Sci U S A* **101**, 14889–14894.

Pal, R., Reitz, M. S., Jr, Tschachler, E., Gallo, R. C., Sarngadharan, M. G. & Veronese, F. D. (1990). Myristoylation of gag proteins of HIV-1 plays an important role in virus assembly. *AIDS Res Hum Retroviruses* **6**, 721–730.

Provitera, P., El-Maghrabi, R. & Scarlata, S. (2006). The effect of HIV-1 Gag myristoylation on membrane binding. *Biophys Chem* **119**, 23–32.

Rhee, S. G. (2001). Regulation of phosphoinositide-specific phospholipase C. *Annu Rev Biochem* **70**, 281–312.

Saad, J. S., Miller, J., Tai, J., Kim, A., Ghanam, R. H. & Summers, M. F. (2006). Structural basis for targeting HIV-1 Gag proteins to the plasma membrane for virus assembly. *Proc Natl Acad Sci U S A* **103**, 11364–11369.

Scholz, I., Still, A., Dhenub, T. C., Coday, K., Webb, M. & Barklis, E. (2008). Analysis of human immunodeficiency virus matrix domain replacements. *Virology* **371**, 322–335.

Stauffer, T. P., Ahn, S. & Meyer, T. (1998). Receptor-induced transient reduction in plasma membrane PtdIns(4,5)P2 concentration monitored in living cells. *Curr Biol* **8**, 343–346.

Swanstrom, R. & Wills, J. W. (1997). Synthesis, assembly, and processing of viral proteins. In *Retroviruses*, pp. 263–334. Edited by J. M. Coffin, S. H. Hughes & H. Varmus. Cold Spring Harbor: Cold Spring Harbor Laboratory Press.

Tall, E. G., Spector, I., Pentyala, S. N., Bitter, I. & Rebecchi, M. J. (2000). Dynamics of phosphatidylinositol 4,5-bisphosphate in actin-rich structures. *Curr Biol* **10**, 743–746.

Wagner, R., Graf, M., Bieler, K., Wolf, H., Grunwald, T., Foley, P. & Uberla, K. (2000). Rev-independent expression of synthetic *gag-pol* genes of human immunodeficiency virus type 1 and simian immunodeficiency virus: implications for the safety of lentiviral vectors. *Hum Gene Ther* **11**, 2403–2413.

Wang, C. T., Zhang, Y., McDermott, J. & Barklis, E. (1993). Conditional infectivity of a human immunodeficiency virus matrix domain deletion mutant. *J Virol* **67**, 7067–7076.

Yagisawa, H., Hirata, M., Kanematsu, T., Watanabe, Y., Ozaki, S., Sakuma, K., Tanaka, H., Yabuta, N., Kamata, H. & other authors (1994). Expression and characterization of an inositol 1,4,5-trisphosphate binding domain of phosphatidylinositol-specific phospholipase C-δ1. *J Biol Chem* **269**, 20179–20188.

Zhou, W., Parent, L. J., Wills, J. W. & Resh, M. D. (1994). Identification of a membrane-binding domain within the amino-terminal region of human immunodeficiency virus type 1 Gag protein which interacts with acidic phospholipids. *J Virol* **68**, 2556–2569.

Separate elements are required for ligand-dependent and -independent internalization of metastatic potentiator CXCR4

Yuko Futahashi,[1] Jun Komano,[1,4] Emiko Urano,[1] Toru Aoki,[1,2] Makiko Hamatake,[1] Kosuke Miyauchi,[1] Takeshi Yoshida,[3] Yoshio Koyanagi,[3] Zene Matsuda[1] and Naoki Yamamoto[1,2]

[1]AIDS Research Center, National Institute of Infectious Diseases, 1-23-1 Toyama, Shinjuku, Tokyo 162-8640; [2]Department of Molecular Virology, Tokyo Medical and Dental University, 1-5-45, Yushima, Bunkyo-ku, Tokyo 113-8519; [3]Laboratory of Viral Pathogenesis, Institute for Virus Research, Kyoto University, 53 Shougoin-kawahara machi, Sakyou-ku, Kyoto 606-8507, Japan

(Received September 17, 2006/Revised November 3, 2006/Accepted November 11, 2006/Online publication January 19, 2007)

The C-terminal cytoplasmic domain of the metastatic potentiator CXCR4 regulates its function and spatiotemporal expression. However, little is known about the mechanism underlying constitutive internalization of CXCR4 compared to internalization mediated by its ligand, stromal cell-derived factor-1 alpha (SDF-1α)/CXCL12. We established a system to analyze the role of the CXCR4 cytoplasmic tail in steady-state internalization using the NP2 cell line, which lacks endogenous CXCR4 and SDF-1α. Deleting more than six amino acids from the C-terminus dramatically reduced constitutive internalization of CXCR4. Alanine substitution mutations revealed that three of those amino acids Ser^{344} Glu^{345} Ser^{346} are essential for efficient steady-state internalization of CXCR4. Mutating Glu^{345} to Asp did not disrupt internalization, suggesting that the steady-state internalization motif is S(E/D)S. When responses to SDF-1α were tested, cells expressing CXCR4 mutants lacking the C-terminal 10, 14, 22, 31 or 44 amino acids did not show downregulation of cell surface CXCR4 or the cell migration induced by SDF-1α. Interestingly, however, we identified two mutants, one with E344A mutation and the other lacking the C-terminal 17 amino acids, that were defective in constitutive internalization but competent in ligand-promoted internalization and cell migration. These data demonstrate that ligand-dependent and -independent internalization is genetically separable and that, between amino acids 336 and 342, there is a negative regulatory element for ligand-promoted internalization. Potential involvement of this novel motif in cancer metastasis and other CXCR4-associated disorders such as warts, hypogammaglobulinemia, infections and myelokathexis (WHIM) syndrome is discussed. (*Cancer Sci* 2007; 98: 373–379)

The chemokine receptor CXCR4 is a class-A G protein-coupled receptor (GPCR; reviewed in [1,2]) and its natural ligand is stromal cell-derived factor-1 alpha (SDF-1α)/CXCL12. CXCR4 also serves as the receptor for HIV type 1 (HIV-1). Many cell types express CXCR4, including peripheral blood lymphocytes, monocytes-macrophages, thymocytes, dendritic cells, endothelial cells, epithelium-derived tumor cells, microglial cells, neurons and hematopoietic stem cells. CXCR4 plays multiple biological roles from promoting development of neuronal networks to regulating migration of leukocytes, cerebellar granule cells and hematopoietic stem cells.[3–8] Analysis of knockout mice indicates that the CXCR4/SDF-1α system is essential for maintenance of hematopoiesis and intestinal vascularization.[9,10]

The CXCR4/SDF-1α system also functions in pathological processes, including autoimmune diseases, cancer progression and metastasis, and AIDS caused by HIV-1. Recently, metastasis of breast cancer cells was found to be regulated by the CXCR4/SDF-1α axis.[5] Similarly, other studies have found that metastasis of other malignancies was controlled by the CXCR4/SDF-1α system, including colon carcinoma[11] non-small cell lung cancer[12] and prostate cancer.[13] These observations suggest that the CXCR4/SDF-1α axis is a potential target for metastatic cancer therapy.

Warts, hypogammaglobulinemia, infections and myelokathexis (WHIM) syndrome is a rare combined immunodeficiency characterized by an unusual form of neutropenia. It is reported that the CXCR4 cytoplasmic tail is mutated and often truncated in WHIM syndrome.[14] Thus, determining the biochemical activity of the CXCR4 cytoplasmic tail should facilitate understanding of the pathogenesis of WHIM syndrome as well as suggest ways to control cancer metastasis.

Following SDF-1α binding, CXCR4 is activated, triggering multiple signaling cascades via Gα or β-arrestin 2 (reviewed in[15]). To desensitize activated CXCR4, the G protein-coupled receptor kinase (GRK) is recruited and phosphorylates serine residues on the CXCR4 cytoplasmic tail, thereby inactivating Gα-mediated signal. Simultaneously, CXCR4 is internalized in a clathrin-dependent manner. β-arrestin 2 competes with Gα for CXCR4 binding and can initiate signal transduction independent from Gα. β-arrestin 2 can also induce clathrin-dependent CXCR4 endocytosis. Thus, cell surface levels of CXCR4 transiently decrease after agonist binding but, several hours later, surface levels of CXCR4 return to normal. Most internalized CXCR4 is transported to lysosomes and degraded, but some internalized CXCR4 is recycled. It is reported that amino acids within the cytoplasmic tail are required for agonist-dependent endocytosis of CXCR4.[16–18]

By contrast, it is unclear how steady-state cell surface levels of CXCR4 are maintained in the absence of SDF-1α. Although cell surface levels of CXCR4 could be regulated at the transcriptional level, it is likely that primary regulation occurs post-translationally. Given that the cell surface levels of CXCR4 are positively correlated with cancer cells' ability to metastasize,[5,19] understanding the post-translational behavior of CXCR4 is likely to shed light on metastatic processes. Historically, cells expressing endogenous CXCR4 have been used for analysis of CXCR4 trafficking. However, as is the case with many G protein-coupled receptors (GPCR), CXCR4 trafficking is influenced by spontaneous oligomerization in the absence of ligand.[20–22] Thus, previous observations might not correctly model phenotypes seen in CXCR4 mutants.

In the present study, we analyzed the contribution of the cytoplasmic tail to the post-translational trafficking of CXCR4 in a cell line lacking both endogenous CXCR4 and SDF-1α. Using genetic approaches, we identified two amino acid motifs within the CXCR4 cytoplasmic tail; one that positively regulates

[4]To whom correspondence should be addressed. E-mail:ajkomano@nih.go.jp

doi: 10.1111/j.1349-7006.2007.00388.x

spontaneous ligand-independent internalization and the other that negatively regulates ligand-dependent CXCR4 internalization.

Materials and methods

Cells. The glioblastoma cell line NP2, human embryonic kidney (HEK) 293T, and HeLa, cells were maintained in RPMI-1640 (Sigma, Tokyo, Japan) supplemented with 10% FBS (Japan Bioserum, Tokyo, Japan), penicillin and streptomycin (Invitrogen, Tokyo, Japan). All cell lines were incubated at 37°C in the humidified 5% CO_2 atmosphere.

Plasmids. Full-length CXCR4 cDNA was amplified from a plasmid kindly provided by Dr Shioda[23] using the following primers: sense, 5′-ACCGGTGCCACCATGGAGGGGATCAGT-ATATACACTTCAG-3′, and antisense, 5′-AGATCTCGCTGGA-GTGAAAACTTGAAGACTCAGACTC-3′. CXCR4 lacking the cytoplasmic tail (d-44) was amplified using the same sense primer and the antisense primer, 5′-AGATCTTGGCTCCAAGGAAA-GCATAGAGGATGGG-3′. Polymerase chain reaction (PCR) fragments were cloned into the *Age* I-*Bgl* II sites of pEGFP-C2 (Clontech, Palo Alto, CA, USA) to create pCXCR4 FL and pCXCR4 d-44, respectively. To construct pCXCR4 FL- and d-44-GFP, the *Sna* BI-*Bgl* II fragments from pCXCR4 FL and d-44 were cloned into the *Sna* BI-*Bgl* II sites of pEGFP-N2, respectively (Clontech). To construct pCXCR4 FL- and d-44-GFP flag, the *Sna* BI-*Bgl* II fragments from pCXCR4 FL and d-44 were cloned into the *Sna* BI-*Bgl* II sites of pEGFP-flag in which the following annealed oligonucleotides had been inserted into the *Bsr* GI site of pEGFP-N2: forward, 5′-GTACGACTAC-AAAGACGATGACGACTATAAGTAAGC-3′, and reverse, 5′-GGCCGCTTACTTATAGTCGTCATCGTCTTTGTAGTC-3′. To construct pCMMP CXCR4 FL- and d-44-GFP, pCXCR4 FL- and d-44-GFP were digested with *Not* I, blunted using T4 DNA polymerase, and further digested with *Age* I. The Age *I*-blunted *Not* I fragments of both constructs were cloned into the pCMMP eGFP plasmid that had been digested with *Bam* HI, blunted with T4 DNA polymerase, and digested with *Age* I. pCMMP CXCR4 FL- and d-44-GFP-flag were constructed using the same strategy. CXCR4 deletion and point mutants were PCR-amplified using the sense primer 5′-ACCGGTGCCACCATGGAGGGGATCAGTG-TGAAAACTTGAAGACTCAGACTC-3′ and the following reverse primers: d-6, 5′-AAGCTTGAGCTCGAGATCTCAG-ACTCAGACTCAGTGGAAAC-3′; d-10, 5′-AAGCTTGAGC-TCGAGATCTCAGTGGAAACAGATGAATGTCC-3′; d-14, 5′-AAGCTTGAGCTCGAGATCTCTGAATGTCCACCTCGC-TTTCC-3′; d-17, 5′-AAGCTTGAGCTCGAGATCTCACCTC-GCTTTCCTTTGG-3′; d-22, 5′-AAGCTTGAGCTCGAGATCT-CGGAGAGGATCTTGAGGCTGGACC-3′; d-31, 5′-AAGCTT-GAGCTCGAGATCTCGCTCACAGAGGTGAGTGCGTGC-3′; E343A, 5′-CGAGATCTCGCTGGAGTGAAAACTTGAAGAC-TCAGACGCAGTGGAAACAGATGAATGTC-3′; S344A, 5′-CGAGATCTCGCTGGAGTGAAAACTTGAAGACTCAGCCT-CAGTGGAAACAGATGAATGTC-3′; E345A, 5′-CGAGATC-TCGCTGGAGTGAAAACTTGAAGACGCAGACTCAGTGGA-AACAGATGAATGTC-3′; S346A, 5′-CGAGATCTCGCTGGA-GTGAAAACTTGAAGCCTCAGACTCAGTGGAAACAGATG-AATGTC-3′; S347E, 5′-CGAGATCTCGCTGGAGTGAAAA-CTTTCAGACTCAGACTCAGTGGAAACAGATGAATGTC-3′; H350E, 5′-CGAGATCTCGCTGGACTCAAAACTTGAAGAC-TCAGACTCAGTGGAAACAGATGAATGTC-3′; S347E/H350E, 5′-CGAGATCTCGCTGGACTCAAAACTTTCAGACTCAGA-CTCAGTGGAAACAGATGAATGTC-3′; and E343/345D, 5′-CGAGATCTCGCTGGAGTGAAAACTTGAAGAGTCAGAGT CAGTGGAAACAGATGAATGTC-3′. The PCR fragments were cloned into the *Age* I-*Bgl* II sites of pCMMP CXCR4 FL-GFP-flag, replacing wild-type with mutant CXCR4. Protein expression of each mutant in 293T cells was verified by Western blot analysis.

Immunoblotting. Immunoblotting was performed as described.[24,25] The primary antibody was anti-green fluorescent protein (GFP) polyclonal antibody (Beckton Dickinson, San Jose, CA, USA). The secondary probe was EnVision+ (Dako, Glostrup, Denmark). Signals were visualized with an LAS3000 imager (Fuji Film, Tokyo, Japan) after treating the membranes with the Lumi-Light Western Blotting Substrate (Roche Diagnostics GmbH, Mannheim, Germany).

Flow cytometry. Cells were labeled with anti-CXCR4 antibodies recognizing the N-terminus conjugated with R-phycoerythrin (PE; 2B11, BD Pharmingen, San Diego, CA) or recognizing the second extracellular loop (12G5) conjugated with either PE or PE-Cy5 (Beckton Dickinson) for 30 min at 4°C. Cells were washed once with phosphate-buffered saline (PBS) supplemented with 1% FBS and analyzed by FACS Aria (Beckton Dickinson). To isolate GFP-expressing NP2 cells, cells were infected with murine leukemia virus (MLV)-based retroviral vectors as described.[25] Cells exhibiting similar green fluorescence intensities were gated and sorted by FACS Aria. Efficiency of internalization was measured by comparing mean fluorescence intensities for cell surface CXCR4 detected by a PE-labeled 2B11 monoclonal antibody before and after SDF-1α treatment (200 ng/mL, Peprotech EC, London, UK).

Microscopic analysis and imaging of cells. To judge a phenotype of a CXCR4 mutant, three independent scientists investigated the mutant cell phenotype under a fluorescent microscope (Olympus, Tokyo, Japan). Each scientist investigated more than 1000 cells for each mutant. More than 99% of cells of a mutant fell in the indicated phenotypic category. These phenotypes were unchanged for more than a year of continuous cultivation in tissue culture. For imaging, NP2 cells were grown on glass plates for more than 24 h, fixed in 4% formaldehyde in PBS for 5 min, stained with Hoechst 33258, mounted (Vectorshield, Vector Laboratories, Burlingame, CA, USA), and imaged using a confocal microscope META 510 (Carl Zeiss, Tokyo, Japan). A representative cell for each CXCR4 mutant carrying a wide cytoplasm was chosen such that the spatial resolution was high. The focal plane just above the glass surface was scanned with an optical thickness of approximately 1 μm. For the imaging of subcellular compartments, cells were incubated with either BODIPY TR ceramid, ER-Tracker Blue-White DPX, or Lysotracker Red DND-99 (Invitrogen) according to the manufacturer's protocol and imaged without fixation. Image brightness and contrast were processed by META510 software (Carl Zeiss). Unless noted, cells were imaged at ×630 magnification, the GFP signal was displayed in green, and Hoechst 33258-stained nuclei were blue. To visualize ligand-induced internalization, cells were treated with 200 ng/mL SDF-1α before fixation. The live cell imaging was performed using Leica DFC350FX system and the images were processed by FW4000 software (Leica Microsystems, Tokyo, Japan). Cells were plated on the glass-bottomed dish (Matsunami glass, Kishiwada, Japan) and incubated at 37°C in the humidified 5% CO_2 atmosphere during the monitoring.

Cell migration assay. Cell migration was measured using an HTS FluoroBlok Multiwell Insert System (8.0 μm pore size, BD Falcon) according to the manufacturer's protocol. For stimulation assays, cells were incubated without serum overnight before SDF-1α treatment (200 ng/mL). Cells were allowed to migrate overnight.

Statistical analysis. Significance of differences were determined by a Student's *t*-test. *P*-values less than 0.05 were considered significant.

RESULTS

Deleting 10 amino acids from the carboxyl end of CXCR4 alters the efficiency of constitutive internalization. Previous studies indicated that the cytoplasmic tail of CXCR4 amino acids 308–352 plays

doi: 10.1111/j.1349-7006.2007.00388.x

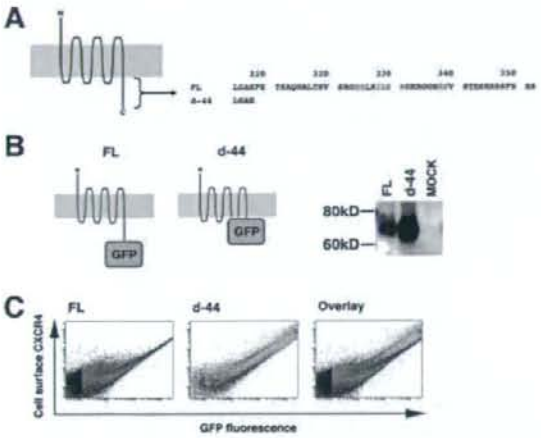

Fig. 1. The effect of stromal cell-derived factor-1 alpha (SDF-1α) treatment on NP2 cells expressing CXCR4 mutants. (a) Cells expressing d-17 were treated with SDF-1α, incubated at 37°C for the indicated times, fixed and imaged. The blue signal represents the Hoechst-stained nucleus. (Original magnification, ×630; bar, 10 μm). (b) FACS analysis to measure internalization efficiency of cell surface CXCR4 and mutant forms 2 h after SDF-1α exposure. The average and standard deviation from the indicated number of independent experiments are shown. Asterisks represent statistically significant difference from the FL levels ($P < 0.01$). (c) Cell migration assay to assess response of cells expressing CXCR4 and mutants to SDF-1α. The number of migrated cells in three to six randomly selected fields was counted and the average and standard deviation were calculated. (□) number of migrated cells in the absence of ligand; (■) migration in the presence of ligand. (*) statistically significant differences in the number of migrated cells between SDF-1α-untreated and -treated cells ($P < 0.01$).

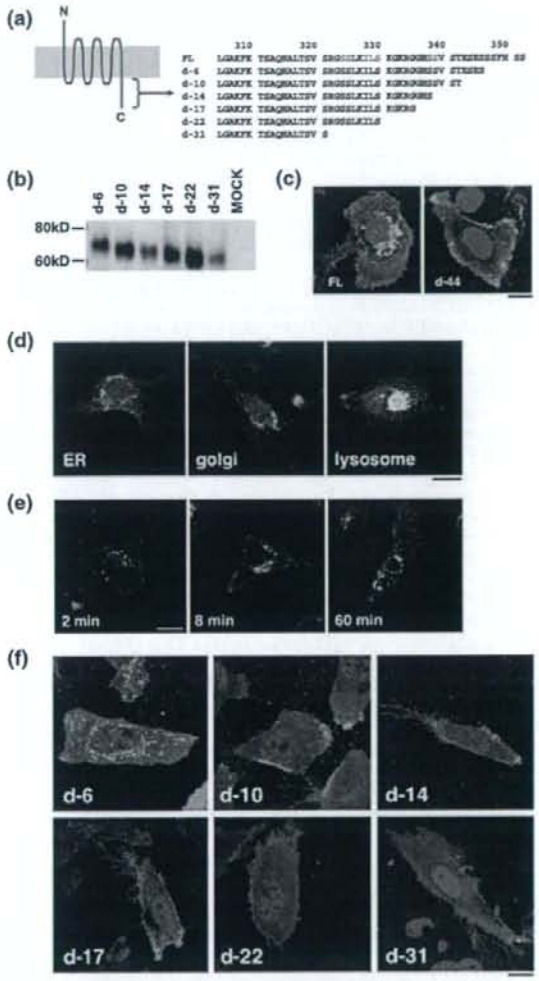

Fig. 2. Expression profiles of CXCR4 and a mutant with cytoplasmic tail deletion. (a) Schematic representation of CXCR4. The N-terminus CXCR4 is exposed in the extracellular space and the C-terminus is intracellular. Gray represents the lipid bilayer. The amino acid sequence of the cytoplasmic tail is shown. Residues in red are required for ligand-induced endocytosis. The CXCR4 d-44 mutant lacks amino acid 309–351. (b) Schematic representation and Western blot of FL and d-44 constructs. (c) Flow cytometry profiles of FL and d-44 expressed in 293T cells. The horizontal axis represents green fluorescence intensity indicative of green fluorescent protein (GFP)-tagged CXCR4 protein levels, and the vertical axis is PE-Cy5 fluorescence intensity, reflecting cell surface CXCR4 detected by the anti-CXCR4 antibody. GFP-positive cells expressing FL are colored in red (left) and those expressing d-44 in green (middle). The expressional differences between FL and d-44 is highlighted on the overlay plot (right).

a critical role in ligand-dependent internalization (Fig. 1a). Also, it has been shown in transfected cells that cell surface levels of CXCR4 lacking the cytoplasmic tail (equivalent to the d-44 mutant here) are higher than those of the full length, wild-type protein (hereafter designated FL), suggesting that the cytoplasmic tail of CXCR4 regulates steady-state internalization.[26,27] To confirm this, we constructed expression plasmids of CXCR4 FL and d-44 fused to GFP or GFP-FLAG at the C-terminus. Previous studies and data reported here indicated that CXCR4 function is not affected by this modification.[28] The expression of each construct was verified by Western blot analysis (Fig. 1b). Single cell-based quantitative analyzes revealed that the ratio of cell surface levels to the total amount of CXCR4 FL (Fig. 1c, left) was consistently lower than that of d-44 (Fig. 1c, middle) at any expression levels (Fig. 1c, right for the comparison). These data supported previous findings and demonstrate that constitutive internalization occurs at any level of CXCR4 expression.

To further examine the contribution of the cytoplasmic tail to post-translational trafficking of CXCR4, we devised a system utilizing the human NP2 glioma line: NP2 cells are flat and exhibit a large cytoplasmic space such that intracellular compartments can be well resolved under the microscope. NP2 cells also lack endogenous CXCR4[29] and SDF-1α (data not shown), both of which could potentially affect distribution of transduced CXCR4. However, NP2 cells are capable of appropriate signaling in response to CXCR4/SDF-1α interaction. We generated a series of CXCR4 deletion mutants lacking the cytoplasmic tail (Fig. 2a) and transduced them into NP2 cells using MLV vectors. Cells bearing similar green fluorescence intensities were collected by FACS sorter. The expression of each mutant was verified by Western blot analysis (Fig. 2b). Microscopic observations revealed that cells expressing FL were bordered by green fluorescence, and significant green fluorescence was detected in vesicular compartments of varying diameters lying close to the nucleus surrounding the nucleus (hereafter designated the FL phenotype, Fig. 2c, left). Vesicles around the nucleus were

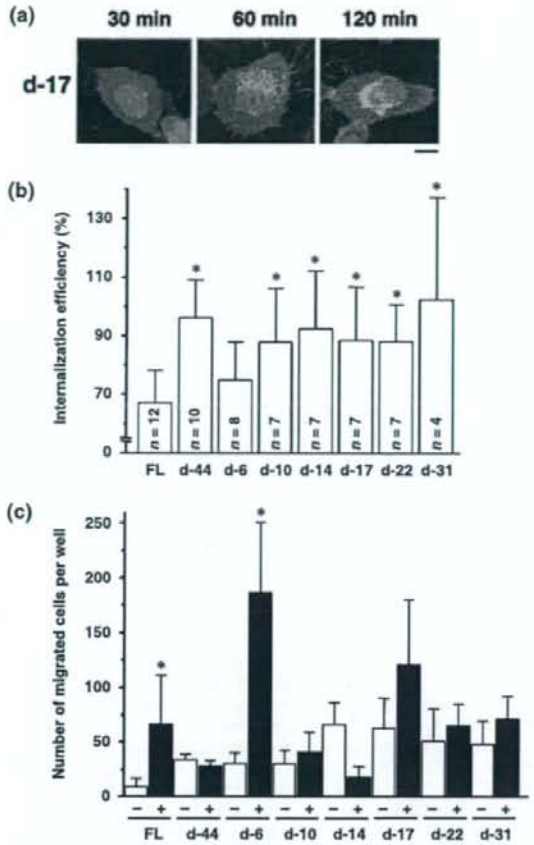

Fig. 3. Identification of the amino acids required for steady-state CXCR4 internalization. (a) Amino acid sequences of the cytoplasmic tail of FL and deletion mutants. Residues in red are required for ligand-induced endocytosis. (b) The protein expression of each mutant in 293T cells was verified by Western blot analysis. (c) Confocal micrographs of NP2 cells expressing FL and d-44 mutant proteins. The blue signal represents the Hoechst-stained nucleus. (Original magnification, ×630; bar, 10 μm.) (d) Confocal micrographs showing NP2 cells expressing CXCR4 FL stained with ER, Golgi, or lysosome organella markers. The organella marker signal is shown in red, the GFP signal is in green. The pixels that both red and green signals co-localized are shown in yellow. (Original magnification, ×630; bar, 10 μm.) (e) CXCR4 FL trafficking in the absence of SDF-1α in NP2 cells. Cell surface CXCR4 FL was labeled with an antibody conjugated with PE-Cy5 (red), incubated at 37°C for the indicated times, fixed and imaged. (Original magnification, ×630; bar, 10 μm.) (f) Confocal micrographs of NP2 cells expressing FL and mutant proteins. The intracellular vesicular green fluorescence reflecting steady-state internalization can be seen in the d-6 mutant. The blue signal represents the Hoechst-stained nucleus. (Original magnification, ×630; bar, 10 μm.)

mostly lysosomes, as demonstrated by fluorescent organella marker analyses in which cells expressing CXCR4 FL-GFP stained with the lysosomal marker yielded a substantial amount of co-localization signal. On the other hand, only a mall amount of co-localization signal was detected when the ER or Golgi markers were used (Fig. 2d), consistent with our biochemical fractionation (unpublished data) and previous publications.[16,27,28,30] The active constitutive internalization was visualized by labeling cell surface CXCR4 by PE-Cy5-conjugated monoclonal antibody followed by fluorescence imaging after cells were incubated at 37°C (Fig. 2e). The live cell imaging revealed that internalizing GFP-positive vesicles trafficked at an average velocity of 4.7 mm/h ($n = 15$), which is within the range of clathrin-dependent vesicular transport (2–20 mm/h), not that of caveolin-dependent vesicular transport (25–170 mm/h).[31–35] These data suggest that the FL is constitutively internalized from the cell surface to the cytoplasmic compartment. In sharp contrast, most green fluorescent signals from d-44 mutant-expressing cells were detected at the cell surface, and only a few small GFP-positive vesicles were seen in the cytoplasm near the nucleus (hereafter designated the d-44 phenotype, Fig. 2c, right). Similar observations were made in d-10, d-14, d-17, d-22 and d-31 mutant-expressing cells (Fig. 2f). The d-6 construct displayed a phenotype similar to FL, although the intracellular GFP signal was less prominent (Fig. 2c). Similar results were obtained in HeLa and 293 cells (data not shown). These data suggest that wild-type CXCR4 was trafficked to the plasma membrane but was internalized spontaneously. Thus, steady-state internalization appeared to be regulated by amino acids located between d-6 and d-10 (e.g. amino acids 343–346).

Steady-state and SDF-1α-induced CXCR4 internalization is genetically separable. Next, we investigated distribution of CXCR4 protein and cell migration after SDF-1α treatment. Confocal analysis showed that after SDF-1α exposure, cells expressing FL, d-6 and d-17 mutants showed GFP signals in intracellular compartments, which were enhanced 60 min after SDF-1α treatment, an effect most clearly shown in d-17-expressing cells (Fig. 3a). GFP signals from intracellular vesicles gradually disappeared 1–2 h after exposure to ligand. Such redistribution of GFP signals was not observed in cells expressing d-10, d-14, d-22, d-31 and d-44 (data not shown). Cell surface levels of CXCR4 before and after SDF-1α treatment were measured by FACS analysis undertaken with an antibody directed against the CXCR4 N-terminus, because that antibody did not interfere with ligand–receptor interaction (Fig. 3b). The downregulation of cell surface levels of FL 2 h after ligand exposure was 67.1 ± 11.1%, whereas that of d-44 was 96.3 ± 12.3% (average and standard deviation from 12 and 10 independent experiments, respectively), consistent with previous reports.[17,27,28] Ligand-induced downregulation of d-6 was 74.9 ± 12.9% ($n = 8$), similar to FL levels. Ligand-induced internalization was significantly less efficient in cells expressing d-10, d-14, d-17, d-22, d-31 and d-44 mutants when compared with FL ($P < 0.001$). Although the d-17 mutant supported ligand-facilitated internalization, as evidenced by microscopic observation, cell surface levels remained unchanged (Fig. 3a,b). This may be due in part to rapid recruitment of newly synthesized d-17 to the cell surface.

Next, we examined cells expressing CXCR4 mutants in response to SDF-1α. Migration results from intracellular signaling initiated by SDF-1α/CXCR4 interaction. Induction of cell migration by SDF-1α in cells expressing FL was 7.2-fold that of untreated cells ($P < 0.05$). In contrast, migration of cells expressing d-44 in response to SDF-1α was undetectable. These data are in agreement with a previous report.[26] The d-6 mutant, which is internalized upon SDF-1α treatment, supported ligand-promoted cell migration by 6.1-fold ($P < 0.01$) relative to untreated cells, similar to FL. Other deletion mutants tested did not display enhanced cell migration following ligand treatment, except for d-17, which showed modestly enhanced (1.9-fold) migration relative to untreated cells, which was not statistically significant. When basal migratory activities were compared, removal of six or more amino acids from the cytoplasmic tail appeared to potentiate migration in the absence of ligand (open bars, Fig. 3c). These data suggest that constitutive internalization is regulated independently of ligand-facilitated internalization.

Identification of CXCR4 S(E/D)S as a ligand-independent internalization motif. The above data indicated that the carboxy-terminal four

doi: 10.1111/j.1349-7006.2007.00388.x

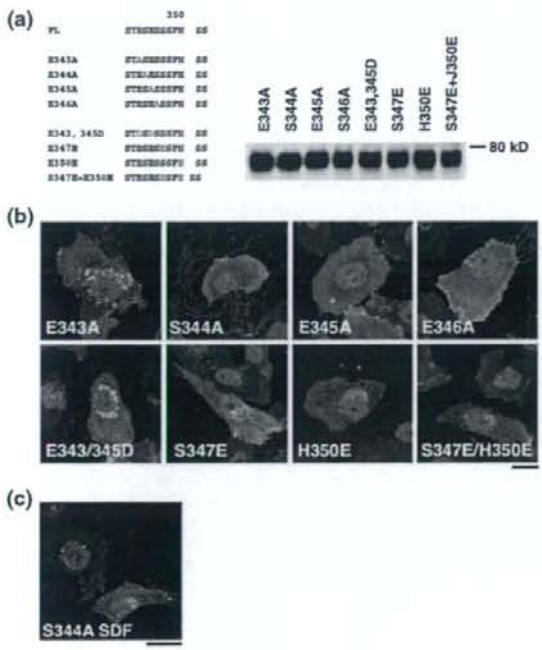

Fig. 4. Characterization of the SDF-1α-independent internalization motif of CXCR4. (a) Left, amino acid sequences of CXCR4 FL and substitution mutants. Letters in red indicate introduced mutations. Right, protein expression of each mutant in 293T cells was verified by Western blot analysis. (b) Confocal micrographs of NP2 cells expressing each mutant. The blue signal represents the Hoechst-stained nucleus. (Original magnification, ×630; bar, 10 μm.) (c) NP2 cells expressing the S344A mutant treated with SDF-1α for 2 h are shown. The blue signal represents the Hoechst-stained nucleus. (Original magnification, ×630; bar, 10 μm.)

amino acids (ESES; residues 343–346) likely function in ligand-independent CXCR4 internalization. To further characterize which amino acids are required for ligand-independent internalization, we generated alanine substitution mutants for each of the four amino acids in the context of FL and examined their phenotypes (Fig. 4a). Protein expression of mutants was verified in Western blot analysis (Fig. 4a). Among the four mutants, the E343A mutant showed the FL phenotype, while the others displayed the d-44 phenotype in the absence of ligand (Fig. 4b). These data demonstrate that Ser^{344}-Glu^{345}-Ser^{346} constitute the core motif for SDF-1α-independent CXCR4 internalization. Both E345A and S346A mutants exhibited the Thr^{342}-Glu^{343}-Ser^{344} sequence adjacent to the original SES sequence. However, this 'SES-like' motif did not support constitutive internalization, suggesting that Thr cannot substitute for Ser to maintain functionality as a constitutive internalization motif. We reasoned that if such a motif requires an acidic amino acid between two serine residues, changing Glu to Asp should maintain the motif's function. Thus, we constructed a mutant in which Glu was replaced with Asp (E343/345D; Fig. 4a). Also, to determine whether two adjacent SES sequences could augment the FL phenotype, we substituted Ser^{347} with Glu (S347E), creating an additional SES motif next to the original SES one (Fig. 4a). As controls, we created H350E and S347E/H350E mutants (Fig. 4a). Expression of these mutants was verified by Western blot analysis (Fig. 4a). Interestingly, the E343/345D mutant retained the FL phenotype (Fig. 4b), indicating that an acidic residue is required to maintain function of the constitutive internalization motif. S347E showed an intermediate phenotype in which numerous fine GFP-positive vesicles were seen close to the nucleus (Fig. 4b). These data indicate that the two adjacent SES sequences do not augment the FL phenotype but actually interfere with steady-state internalization. Both H350E and S347E/H350E mutants also showed an intermediate phenotype (Fig. 4b), suggesting that more than three acidic amino acids close to the SES motif may inhibit its function, potentially by generating a negative charge cluster. Overall, we conclude that the SDF-1α-independent internalization motif is located at amino acids 344–346 of the CXCR4 cytoplasmic tail.

Finally, we analyzed phenotypes of the S344A mutant in greater detail. Two hours after SDF-1α treatment, cells expressing this mutant showed accumulation of GFP signals at perinuclear regions, similar to the d-17 mutant (Figs. 1a and 4c). FACS analysis revealed that cell surface levels of S344A decreased to $70.8 \pm 11.7\%$ ($n = 7$) following SDF-1α treatment relative to untreated cells, almost as efficient as FL (Fig. 3b). Migratory activity of cells expressing the S344A mutant was stimulated 3.0-fold by SDF-1α, while that of cells expressing FL assayed in parallel showed a 5.8-fold increase relative to untreated cells. These data demonstrate that the S344A mutant, which is defective in constitutive internalization, can undergo ligand-dependent internalization and stimulate migration. Along with the d-17 data, our observations strongly suggest that genetic elements required for the ligand-dependent and -independent internalization are separable.

Discussion

We demonstrated here that CXCR4 is constitutively internalized in the absence of SDF-1α and that steady-state trafficking of CXCR4 is regulated by its cytoplasmic tail. We show that the three amino acid motif, Ser^{344}-Glu^{345}-Ser^{346}, within the cytoplasmic tail is essential for efficient steady-state internalization of CXCR4. Our work indicates that ligand-independent internalization of CXCR4 is genetically separable from ligand-dependent internalization: mutants defective in steady-state internalization (d-17 and S344A) were competent to respond to SDF-1α-promoted internalization signals. That residues required for ligand-dependent endocytosis (Ser324, 325, 330, 338, 339, Ile^{328} Leu^{329} and Lys^{331}; summarized in Fig. 1a)[16–18] do not overlap with those required for ligand-independent internalization, further supports the idea that these activities are separable.

Interestingly, the d-17 mutant displayed SDF-1α-promoted internalization, whereas the d-14 and d-22 mutants did not. These data suggest that an element between amino acids 336 and 342 negatively regulates ligand-initiated CXCR4 internalization. We are currently determining what amino acids are required for that motif. What is unique about the constitutive internalization motif is its position effect in terms of the distance of the motif from the "body" of the receptor. SES-like motifs can be found in the cytoplasmic tails of both CXC-chemokine receptors (for example, CXCR3) and CC-chemokine receptors including CCR2, CCR5 and CCR7. Indeed, these receptors share similar amino acid sequences in which two acidic amino acids (mostly Asp) positioned between the 36th and 45th amino acids of the cytoplasmic tail, where Ser and Thr residues are often in the close proximity to the acidic amino acids but positively charged amino acids, are infrequent. We hypothesize that for the ligand-independent internalization motif to function, the SES motif or its equivalent must be positioned at approximately the 40th residue of the cytoplasmic tail.

Many GPCR, including α1a-adrenoceptor, and the μ-opioid receptor, are spontaneously internalized.[36,37] Therefore, we conclude that various GPCR actively and continuously undergo endocytosis in the absence of ligand in a manner similar to

CXCR4 and hypothesize that the function of constitutive receptor internalization is to fine-tune the threshold at which cells sense ligand. Cells should be able to rapidly post up- and downregulate cell surface levels of CXCR4 using post-translational mechanisms. Such regulation should enable cells to migrate toward SDF-1α-rich tissues as needed and should also prevent inappropriate cells from migrating.

Our work is relevant to cancer cell metastasis and the pathogenesis of WHIM syndrome. Cell surface levels of CXCR4 positively correlate with cancer cells' ability to metastasize.[5,19] We hypothesize that enhanced metastatic capabilities of cancer cells could be due in part to mutations that disrupt the function of SES motif, which would result in upregulation of cell surface levels of signal-competent CXCR4 (as exemplified by the E344A mutant). As for WHIM syndrome, it was recently reported that it is due to mutations within CXCR4's cytoplasmic domain.[14,38] Interestingly, these mutations result in loss of SES motif. We predict that loss of the SES motif should increase cell surface CXCR4 levels. Although CXCR4 mutations generated here are not identical to reported WHIM mutations, the d-10 mutant resembles mutations seen in WHIM syndrome, and it exhibits enhanced basal cell migratory activity. Increased cell surface CXCR4 or increased migratory potential may contribute to WHIM pathogenesis. The response of d-10-expressing cells to SDF-1α, however, was not as robust as that of cells derived from WHIM.[39,40] This discordance may be partly due to the cell type differences, as we have employed a glioblastoma cell line for our studies.

Thus, CXCR4 is a potentially important therapeutic target not only for cancers but for other conditions such as HIV-1 infection, chronic autoimmune disease, and genetic disorders including WHIM syndrome. CXCR4 also plays critical roles in embryogenesis, homeostasis and inflammation. Although there are potential caveats for treating cancer with CXCR4 antagonists, our data furthers the understanding of mechanisms regulating CXCR4 and could be useful in devising therapeutic strategies.

Acknowledgments

We thank Drs Toshitada Takemori and Tsutomu Murakami for critical reading of the manuscript. This work was supported in part by the Japan Human Science Foundation, the Japanese Ministry of Health, Labor and Welfare, and the Japanese Ministry of Education, Culture, Sports, Science and Technology.

References

1 Gether U. Uncovering molecular mechanisms involved in activation of G protein-coupled receptors. *Endocr Rev* 2000; **21**: 90–113.
2 Ferguson SS. Evolving concepts in G protein-coupled receptor endocytosis: the role in receptor desensitization and signaling. *Pharmacol Rev* 2001; **53**: 1–24.
3 Sapede D, Rossel M, Dambly-Chaudiere C, Ghysen A. Role of SDF1 chemokine in the development of lateral line efferent and facial motor neurons. *Proc Natl Acad Sci USA* 2005; **102**: 1714–8. Epub 2005 January 19.
4 Coughlan CM, McManus CM *et al.* Expression of multiple functional chemokine receptors and monocyte chemoattractant protein-1 in human neurons. *Neuroscience* 2000; **97**: 591–600.
5 Muller A, Homey B, Soto H *et al.* Involvement of chemokine receptors in breast cancer metastasis. *Nature* 2001; **410**: 50–6.
6 Zou YR, Kottmann AH, Kuroda M, Taniuchi I, Littman DR. Function of the chemokine receptor CXCR4 in haematopoiesis and in cerebellar development. *Nature* 1998; **393**: 595–9.
7 Ma Q, Jones D, Borghesani PR *et al.* Impaired B-lymphopoiesis, myelopoiesis, and derailed cerebellar neuron migration in CXCR4- and SDF-1-deficient mice. *Proc Natl Acad Sci USA* 1998; **95**: 9448–53.
8 Wang JF, Park IW, Groopman JE. Stromal cell-derived factor-1alpha stimulates tyrosine phosphorylation of multiple focal adhesion proteins and induces migration of hematopoietic progenitor cells: roles of phosphoinositide-3 kinase and protein kinase C. *Blood* 2000; **95**: 2505–13.
9 Kawabata K, Ujikawa M, Egawa T *et al.* A cell-autonomous requirement for CXCR4 in long-term lymphoid and myeloid reconstitution. *Proc Natl Acad Sci USA* 1999; **96**: 5663–7.
10 Peled A, Petit I, Kollet O *et al.* Dependence of human stem cell engraftment and repopulation of NOD/SCID mice on CXCR4. *Science* 1999; **283**: 845–8.
11 Zeelenberg IS, Ruuls-Van Stalle L, Roos E. The chemokine receptor CXCR4 is required for outgrowth of colon carcinoma micrometastases. *Cancer Res* 2003; **63**: 3833–9.
12 Phillips RJ, Burdick MD, Lutz M, Belperio JA, Keane MP, Strieter RM. The stromal derived factor-1/CXCL12-CXC chemokine receptor 4 biological axis in non-small cell lung cancer metastases. *Am J Respir Crit Care Med* 2003; **167**: 1676–86.
13 Taichman RS, Cooper C, Keller ET, Pienta KJ, Taichman NS, McCauley LK. Use of the stromal cell-derived factor-1/CXCR4 pathway in prostate cancer metastasis to bone. *Cancer Res* 2002; **62**: 1832–7.
14 Hernandez PA, Gorlin RJ, Lukens JN *et al.* Mutations in the chemokine receptor gene CXCR4 are associated with WHIM syndrome, a combined immunodeficiency disease. *Nat Genet* 2003; **34**: 70–4.
15 Lefkowitz RJ, Shenoy SK. Transduction of receptor signals by beta-arrestins. *Science* 2005; **308**: 512–7.
16 Marchese A, Benovic JL. Agonist-promoted ubiquitination of the G protein-coupled receptor CXCR4 mediates lysosomal sorting. *J Biol Chem* 2001; **276**: 45 509–12.
17 Orsini MJ, Parent JL, Mundell SJ, Benovic JL, Marchese A. Trafficking of the HIV coreceptor CXCR4. Role of arrestins and identification of residues in the c-terminal tail that mediate receptor internalization. *J Biol Chem* 1999; **274**: 31 076–86.
18 Marchese A, Raiborg C, Santini F, Keen JH, Stenmark H, Benovic JL. The E3 ubiquitin ligase AIP4 mediates ubiquitination and sorting of the G protein-coupled receptor CXCR4. *Dev Cell* 2003; **5**: 709–22.
19 Darash-Yahana M, Pikarsky E, Abramovitch R *et al.* Role of high expression levels of CXCR4 in tumor growth, vascularization, and metastasis. *FASEB J* 2004; **18**: 1240–2.
20 Vila-Coro AJ, Rodriguez-Frade JM, Martin De Ana A, Moreno-Ortiz MC, Martinez AC, Mellado M. The chemokine SDF-1alpha triggers CXCR4 receptor dimerization and activates the JAK/STAT pathway. *FASEB J* 1999; **13**: 1699–710.
21 Babcock GJ, Farzan M, Sodroski J. Ligand-independent dimerization of CXCR4, a principal HIV-1 coreceptor. *J Biol Chem* 2003; **278**: 3378–85.
22 Terrillon S, Bouvier M. Roles of G-protein-coupled receptor dimerization. *EMBO Rep* 2004; **5**: 30–4.
23 Hu H, Shioda T, Hori T *et al.* Dissociation of ligand-induced internalization of CXCR-4 from its co-receptor activity for HIV-1 Env-mediated membrane fusion. *Arch Virol* 1998; **143**: 851–61.
24 Yanagida M, Hayano T, Yamauchi Y *et al.* Human fibrillarin forms a sub-complex with splicing factor 2-associated p32, protein arginine methyltransferases, and tubulins alpha 3 and beta 1 that is independent of its association with preribosomal ribonucleoprotein complexes. *J Biol Chem* 2004; **279**: 1607–14.
25 Komano J, Miyauchi K, Matsuda Z, Yamamoto N. Inhibiting the Arp2/3 complex limits infection of both intracellular mature vaccinia virus and primate lentiviruses. *Mol Biol Cell* 2004; **15**: 5197–207.
26 Roland J, Murphy BJ, Ahr B *et al.* Role of the intracellular domains of CXCR4 in SDF-1-mediated signaling. *Blood* 2003; **101**: 399–406.
27 Haribabu B, Richardson RM, Fisher I *et al.* Regulation of human chemokine receptors CXCR4. Role of phosphorylation in desensitization and internalization. *J Biol Chem* 1997; **272**: 28 726–31.
28 Tarasova NI, Stauber RH, Michejda CJ. Spontaneous and ligand-induced trafficking of CXC-chemokine receptor 4. *J Biol Chem* 1998; **273**: 15 883–6.
29 Soda Y, Shimizu N, Jinno A *et al.* Establishment of a new system for determination of coreceptor usages of HIV based on the human glioma NP-2 cell line. *Biochem Biophys Res Commun* 1999; **258**: 313–21.
30 Zhang Y, Foudi A, Geay JF *et al.* Intracellular localization and constitutive endocytosis of CXCR4 in human CD34+ hematopoietic progenitor cells. *Stem Cells* 2004; **22**: 1015–29.
31 Mundy DI, Machleidt T, Ying YS, Anderson RG, Bloom GS. Dual control of caveolar membrane traffic by microtubules and the actin cytoskeleton. *J Cell Sci* 2002; **115**: 4327–39.
32 Rappoport JZ, Taha BW, Lemeer S, Benmerah A, Simon SM. The AP-2 complex is excluded from the dynamic population of plasma membrane-associated clathrin. *J Biol Chem* 2003; **278**: 47 357–60.
33 Rappoport JZ, Simon SM. Real-time analysis of clathrin-mediated endocytosis during cell migration. *J Cell Sci* 2003; **116**: 847–55.
34 Keyel PA, Watkins SC, Traub LM. Endocytic adaptor molecules reveal an endosomal population of clathrin by total internal reflection fluorescence microscopy. *J Biol Chem* 2004; **279**: 13 190–204.
35 Yarar D, Waterman-Storer CM, Schmid SL. A dynamic actin cytoskeleton functions at multiple stages of clathrin-mediated endocytosis. *Mol Biol Cell* 2005; **16**: 964–75.

doi: 10.1111/j.1349-7006.2007.00388.x